REVIEW

Check for updates

Rejuvenation of dearomative cycloaddition reactions *via* visible light energy transfer catalysis

Angshuman Palai,† Pramod Rai† and Biplab Maji ID *

Dearomative cycloaddition is a powerful technique to access sp³-rich three-dimensional structural motifs from simple flat, aromatic feedstock. The building-up of unprecedentedly diverse polycyclic scaffolds with increased saturation and stereochemical information having various applications ranging from pharmaceutical to material sciences, is an essential goal in organic chemistry. However, the requirement of large energy inputs to disrupt the aromaticity of an arene moiety necessitates harsh reaction conditions for ground state dearomative cycloaddition. The photochemical requirement encompasses use of ultraviolet (UV) light to enable the reaction on an excited potential energy surface. The microscopic reversibility under thermal conditions and the use of high energy harmful UV irradiation in photochemical manoeuvres, however, constrain their widespread use from a synthetic point of view. In this context, the recent renaissance of visible light energy transfer (EnT) catalysis has become a powerful tool to initiate dearomative cycloaddition as a greener and more sustainable approach. The excited triplet state population is achieved by triplet energy transfer from the appropriate photosensitizer to the substrate. While employing mild visible light energy as fuel, the process leverages an enormous potential of excited state reactivity. The discovery of an impressive portfolio of organic and inorganic photosensitizers with a range of triplet energies facilitates visible light photosensitized dearomative cycloaddition of various substrates to form sp³-rich fused polycyclic architectures with diverse applications. The tutorial review comprehensively surveys the reawakening of dearomative cycloadditions *via* visible light-mediated energy transfer catalysis in the past five years. The progress ranges from intra- and intermolecular $[2\pi + 2\pi]$ to $[4\pi + 2\pi]$ cycloadditions, and ends at intermolecular $[2\pi + 2\sigma]$ cycloadditions. Furthermore, the review provides potential possibilities for future growth in the growing field of visible light energy transfer catalysis.

1. Introduction

Rapid generation of molecular complexity from readily available starting materials is one of the trickiest approaches in synthetic chemistry. The cycloaddition reactions bring exciting opportunities in this regard due to their perfect atom economy, stereospecificity, and single-step operation.[1,2] Aromatic compounds could, in principle, be ideal reaction partners for cycloaddition reactions, as they, at least from a topological point of view, contain requisite ene-components. Furthermore, the dearomative cycloaddition reactions could be considered an advanced synthetic and practically rewarding tactic for producing polycyclic three-dimensional architectures from widely abundant flat molecules.[3,4] However, the aromatic stability of these conjugated systems must be broken during these reactions, which is translated as kinetic and thermodynamic barriers for these processes.[5–7] Even if the kinetic barrier

can be overcome, the endothermicity of these reactions makes these reactions reversible and favors the starting materials under thermal conditions (Fig. 1A).

Decades of rigorous research have unraveled the panorama of prospective cycloadditions involving fascinating substrate activations.[8] As illustrated in Fig. 1A, the thermal pathway for achieving dearomative cycloadditions is endergonic. This can be attributed to the loss of molecular stability from the loss of aromatic stabilization. The high potential barrier requires the employment of harsher reaction conditions, which, however, favors reversibility, thus giving low yields of the desired cycloadduct. Shifting to photochemical routes (Fig. 1B and C) makes it possible to incite the reactant selectively by judicious choice of light sources of appropriate wavelengths while leaving the product intact.[9] As illustrated in Fig. 1B, a starting material can be selectively excited when the light energy ($h\nu_1$) is matched with the $[\Delta G(S_1) - \Delta G(S_0)]_{SM}$. Thus, the endergonic cycloadduct ($[\Delta G(S_1) - \Delta G(S_0)]_{product} > h\nu_1$) would be trapped kinetically, and the backward thermal retro-cycloaddition reaction can be prevented effectively by negating the principle of microscopic reversibility, keeping the much lower kinetic barrier in view. In

Department of Chemical Sciences, Indian Institute of Science Education and Research Kolkata, Mohanpur 741246, West Bengal, India. E-mail: bm@iiserkol.ac.in

† These two authors contributed equally.
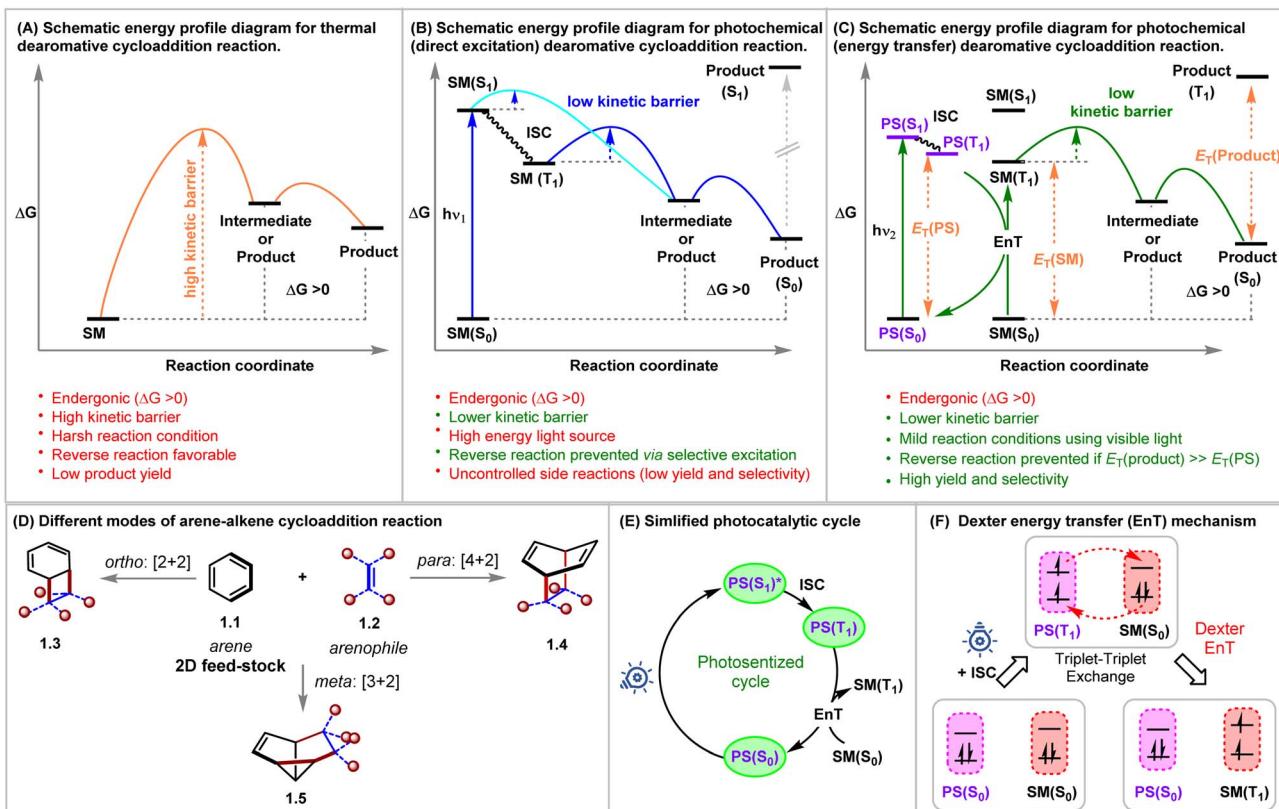
Fig. 1 Schematic energy profile diagram for (A) thermal, (B) UV light-mediated photochemical, and (C) visible light-energy transfer mediated dearomative cycloaddition reactions. (D) Different modes of the arene−alkene cycloaddition reaction. (E) Simplified photocatalytic cycle. (F) Schematic mechanism of Dexter energy transfer (EnT). SM = starting material; PS = photosensitizer; ISC = intersystem crossing; $E_T = \Delta G(T_1) - \Delta G(S_0)$.

this regard, the extent of photochemical reactivity for aromatic compounds ranges from isomerizations, additions, and substitutions to cycloadditions *via* direct excitation of the aromatic chromophore.[3,10] Based on the orbital symmetry and mode of connection, the arene–arenophile cycloaddition can be considered to be of three types: *ortho* [2 + 2], *meta* [3 + 2], and *para* [4 + 2] (Fig. 1D).[3]

The foundation for photochemical dearomative cycloadditions was laid in 1959 with the commencement of the pioneering work on classical *ortho*-cycloaddition by Angus and Bryce-Smith.[11] *Meta*-photocycloaddition was discovered in 1966, independently by Wilzbach and Kaplan.[12] Five years after this unearthing of the *meta*-variant, the same duo realized the *para*-cycloaddition of benzene with olefins forming bicyclo[2.2.2]-octa-2,5-dienes upon irradiation of their reaction mixture at 254 nm.[13] Bryce-Smith later conducted a detailed investigation on the orbital symmetry relationships requisite for *ortho*-, *meta*-, and *para*-cycloadditions of benzene under thermal and photochemical conditions.[14] In 1982, Houk interpreted frontier orbital overlap between benzene and ethylene, revealing that the *ortho*- and *meta*-cycloadditions are photochemically allowed, whereas *para*-cycloaddition is photochemically forbidden.[15] This was in total correlation with the well-established Woodward–Hoffman rule.[16] Bryce-Smith, Gilbert, and Orger raised an open question about the involvement of singlet or triplet intermediates in the existing reports as

molecular orbital symmetry arguments only allow *meta*-cycloadditions to occur in a concerted fashion if benzene's first excited singlet state, *i.e.*, from S_1 benzene ($^1B_{2u}$ = particular concerted process occurring from the lowest excited singlet state in the system; that is from S_1) is involved. Bryce-Smith showed the interaction between the first excited singlet state, *i.e.*, from S_1 of arene ($^1B_{2u}$) and an alkene to be symmetry allowed, whereas the same reaction from the triplet excited state, *i.e.*, T_1 of arene ($^3B_{1u}$ = particular concerted process occurring from the triplet state in the system; that is from T_1) state was symmetry forbidden.[14] Ferree *et al.* provided evidence for the occurrence of *meta*-cycloaddition *via* the singlet excited state only under the influence of direct excitation.[17] The *para*-cycloadduct formation was found to be feasible if either the reaction took place in a non-concerted manner (independent of the Woodward–Hoffmann rule) or *via* the involvement of the second singlet excited state ($^1B_{1u}$ = particular concerted process occurring from the second excited-state of benzene) of benzene.[18] The selectivity of the type of cycloaddition depends on the electronic properties of coupling partners engaged in the process. The Rehm–Weller equation is utilized to draw inferences regarding the reaction mode from the parameters showcasing the possibilities of electron and charge transfer in the excited state (eqn (1)).[19] The free energies (ΔG^{ET}) corresponding to the charge transfer could be calculated from the given equation simply by using the oxidation potential of the donor

$E^{ox}(D)$, the reduction potential of the acceptor $E^{red}(A)$, and the excitation energy of the electronically excited species. According to Mattay, electron-rich and electron-deficient olefin partners preferentially produce the *meta*-cycloadduct with benzene given that $\Delta G^{ET} > 1.4$–1.6 eV and in other cases, give rise to the *ortho*-cycloaddition product. The Weller equation shows that the *meta*- to *ortho*-cycloadduct transition increases upon decreasing the value of ΔG^{ET} below 1.4 eV.[20]

Weller equation: $\Delta G^{ET} = E_{1/2}^{ox}(D) - E_{1/2}^{red}(A) - \Delta E_{excit} + \Delta E_{coul}$ (1)

where ΔG^{ET} = free enthalpy of the radical ion pair formation and $E_{1/2}^{ox,red}$ = half wave potential. D = donor; A = acceptor. ΔE_{excit} = excitation energy of the chromophore. ΔE_{coul} = coulombic interaction energy of the radical ion.

In addition to product selectivity issues discussed above, the use of high-energy UV irradiation is a severe concern for the classic photochemical dearomative cycloaddition reaction.[21,22] Low product yields, low functional group tolerance, and unpredictable side reactions are common characteristics of these methods, posing a limitation on their widespread applicability. As a result, developing mild visible-light-mediated catalytic techniques can serve as an important tool for addressing the problems mentioned above.[23,24]

In this regard, an external photosensitizer (PS) allows aromatic hydrocarbons (ArH) to get photochemically excited by incident visible light energy (Fig. 1C). The PS absorbs the visible light energy to reach its triplet state (T_1) and transfers it to the ArH, a process known as triplet sensitization or energy transfer (EnT), which excites ArH indirectly to its triplet state. A simplified photosensitized cycle is depicted in Fig. 1E. Mechanistically, EnT is classified into three types: primitive EnT, Förster resonance EnT (a radiation-free transmitter-receiver mechanism),[25] and Dexter EnT (Fig. 1F).[26] Dexter described the concurrent two-electron transfer mechanism in 1953 (Fig. 1F).[26] In the context of dearomative cycloaddition reactions in organic synthesis, the photosensitized pathway generally follows the Dexter EnT mechanism, providing mild conditions and establishing the requirement of low activation energy over a thermodynamically unfavorable thermal route. In Dexter EnT, a photochemically excited PS transfers an electron to the lowest unoccupied molecular orbital (LUMO) of the ArH substrate while simultaneously receiving another electron from its highest occupied molecular orbital (HOMO). Excited state energy transfer and spin multiplicity reversal are observed synchronously. The proximity between the PS and the ArH is essential for efficient Dexter EnT, and the rate decays exponentially with the increasing separation between them.[25] The triplet state energy differences $\Delta E_T = E_T(PS) - E_T(ArH)$ can be used to predict the efficiency of Dexter EnT, and the overall efficiency of EnT is co-related with the ΔE_T.[27] When $\Delta E_T > 0$ (exergonic), many coupled transitions are able to populate the substrate's triplet state. When $\Delta E_T < $ (endergonic), coupled transitions only exist from excited vibrational and rotational levels of the PS's triplet state, leading to inefficient triplet-state excitation of the substrates.[28] The overall rate of EnT is determined by using the diffusion rate and the spectral overlap integral, which can be

calculated from the energies of the triplet excited states.[25,29] The product could be kinetically trapped if the $E_T(PS) < E_T(product)$, and the product selectivity can be determined.

An efficient energy transfer catalyst or a PS should have the following characteristics: (1) a large absorption cross-section, (2) an effective intersystem crossing (ISC) to its triplet state, (3) a long excited state lifetime, and (4) high triplet state energy compared to that of the substrate. In 1950, the sensitization-induced synthetic technique was first introduced, in which ketones, with the lowest π^* excited state, acted as the PS.[30] However, the application of said ketones as photosensitizers is quite limited owing to their low absorption at longer wavelengths. Besides, the $n-\pi^*$ transition produces an unpaired electron on the oxygen atom and promotes hydrogen atom transfer (HAT), resulting in unwanted products. Later, ruthenium and iridium-based photocatalysts emerged, demonstrating high visible-light absorption and longer excited state lifetimes.[31]

The triplet state energy transfer (EnT) catalysis has been recently employed for diverse organic transformations and reviewed as well.[23,32–40] The last review focused on arene–alkene cycloaddition was reported in 2016.[3] The modern visible-light mediated EnT dearomative cycloaddition has been advanced since 2018 and is rapidly developing en route to becoming the cornerstone of synthetic methodology. This tutorial article is envisioned to summarize the recent developments to educate the readers and demonstrate the exciting opportunities ahead. The following sections provide an in-depth study and critical analysis of the dearomative cycloaddition of different aromatic compounds and their applications in various sustainable chemical syntheses. The literature is classified based on the mode of connection and sub-categorized based on the intra- and intermolecularity of the cycloadditions involved.

2. Dearomative [2 + 2] *ortho*-cycloaddition

Substantial research has been conducted on arene–alkene [$2\pi + 2\pi$] cycloaddition reactions (Fig. 1D), often referred to as *ortho*-cycloaddition reactions employing direct excitation of the arene by UV irradiation.[3] As discussed, the first *ortho* photocycloaddition of benzene with maleic anhydride was reported by Angus and Bryce-Smith.[11] Since then, this field has received significant contributions from many groups, including Faggiani,[41] Hanzawa and Panqutte,[42] Wagner and Nahm,[43] Zupancic and Sket,[44] and Hoffmann and Pete.[45] The visible-light-induced variant was discovered only recently. Triplet sensitization is employed to excite the arene moiety for a stepwise reaction with the olefin counterpart to produce the cyclobutane fragment, widely present in several natural products, pharmaceuticals, and agrochemicals.[46,47] The following section summarizes the recent developments.

2.1. Intramolecular dearomative [$2\pi + 2\pi$] *ortho*-cycloaddition

In 2018, Glorius *et al.* reported the first visible light-mediated EnT dearomative [2 + 2] cycloaddition reaction (Fig. 2).[48]
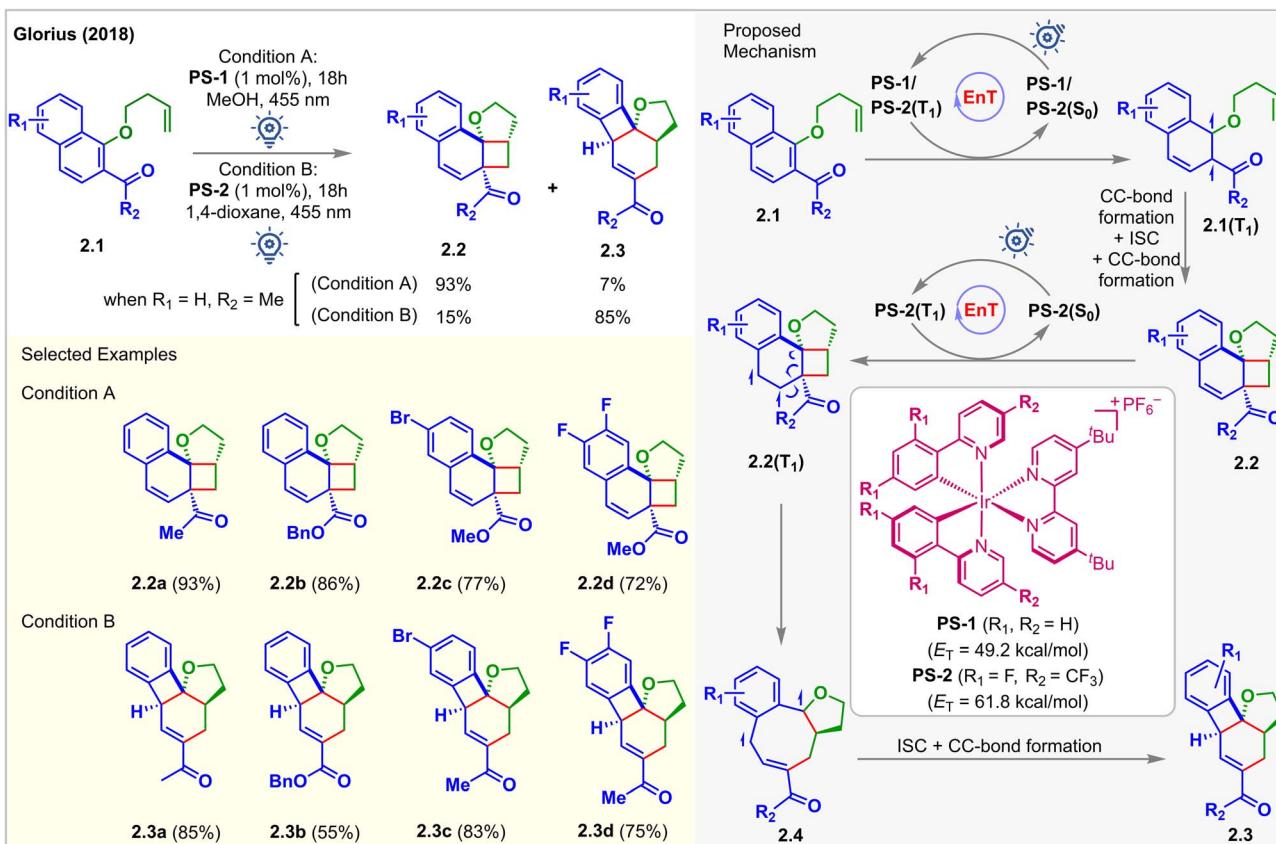
Fig. 2 Visible light mediated EnT dearomative intramolecular [2π + 2π] cycloaddition of alkene-tethered 2-acetyl naphthalene derivatives.

When the iridium-based photosensitizer **PS-1** (E_T = 49.2 kcal mol^{-1}) was irradiated with 455 nm LEDs in MeOH in the presence of the substrates **2.1**, alkene tethered 1-naphthols bearing an adjacent electron-withdrawing group, the [2 + 2] cycloadduct **2.2a** was isolated in 93% yield. However, when **PS-2**, having a higher E_T (=61.8 kcal mol^{-1}), capable of exciting **2.2**, was used, a different cascade product **2.3** with a 6/4/6/5 fused ring structure was isolated. The E_T of **2.2a** was computed to be 55.9 kcal mol^{-1} (B3LYP/6-311+G(2d,p) level of density functional theory (DFT)), and **PS-1** could not productively interact with **2.2a** since it has a low triplet energy of 49.2 kcal mol^{-1}. The consequent experimental studies demonstrated the selective synthesis of [2 + 2] cycloadduct **2.2** using **PS-1** (1 mol%) in 0.02 M MeOH (condition A) and cascade product **2.3** using **PS-2** (1 mol%) in 0.04 M 1,4-dioxane (condition B). A detailed study on the photophysical properties of the PSs confirmed that photoinduced single electron transfer (SET) was not responsible for the generation of **2.2** and **2.3**. Instead, the authors correlated the differing product identities with the different E_Ts of the respective PSs. Both PSs absorbed visible light and became excited to their triplet state, thus activating naphthols **2.1** via EnT to their triplet state **2.1(T$_1$)**, followed by the commencement of intramolecular stepwise [2 + 2] cycloaddition to generate cyclobutanes **2.2**. The selectivity mentioned above was found to be controlled by the relative rates of EnT between the PS and substrate. Stern–Volmer quenching studies showed that

2.2 effectively quenched the luminescence of **PS-2** only. **PS-1** having a lower E_T does not interact with **2.2**. Thus, it was proposed that rapid conversion of **2.1** to **2.2** initially occurred. **2.3** was formed subsequently from **2.2** via EnT-mediated vinyl cyclobutane rearrangement. It should be noted that no reaction was observed in the absence of the electron-withdrawing carbonyl group, which is essential to lower the E_T of the naphthol moiety to undergo EnT with desired efficiency.

The You group was the first to report visible light-mediated EnT intramolecular partial dearomative [2 + 2] cycloaddition of indole derivatives **3.1** bearing a tethered alkene (Fig. 3, condition A).[49] The E_Ts of C2-unsubstituted and unprotected indole derivatives (**3.1**, $R_1 = R_2 = H$) was calculated to be 65 kcal mol^{-1} (B3LYP/6-311+G(2d,p) level of DFT), which bore no parity with the E_Ts of **PS-1** (E_T = 49.2 kcal mol^{-1}) and **PS-2** (E_T = 61.8 kcal mol^{-1}), and thus does not react (yield of **3.2a** = 0%) under the irradiation of visible light. Extending the conjugation by incorporating a Ph group at the C2 position (**3.1**, $R_2 = Ph$) lowered the E_T to 55.9 kcal mol^{-1}. It smoothly underwent the [2 + 2] cycloaddition in the presence of **PS-2** (4 mol%) in a CH$_2$Cl$_2$/CH$_3$CN solvent mixture (3 : 1) to produce cycloadduct **3.2b** with an excellent 95% yield. Notably, the reactivity also increased significantly for the N-electron withdrawing protecting group. The N-trifluoroacetyl indole derivative produced **3.2d** in 98% yield. The proposed mechanism involved the excitation of **PS-2** under blue light irradiation and EnT to yield a diradical species
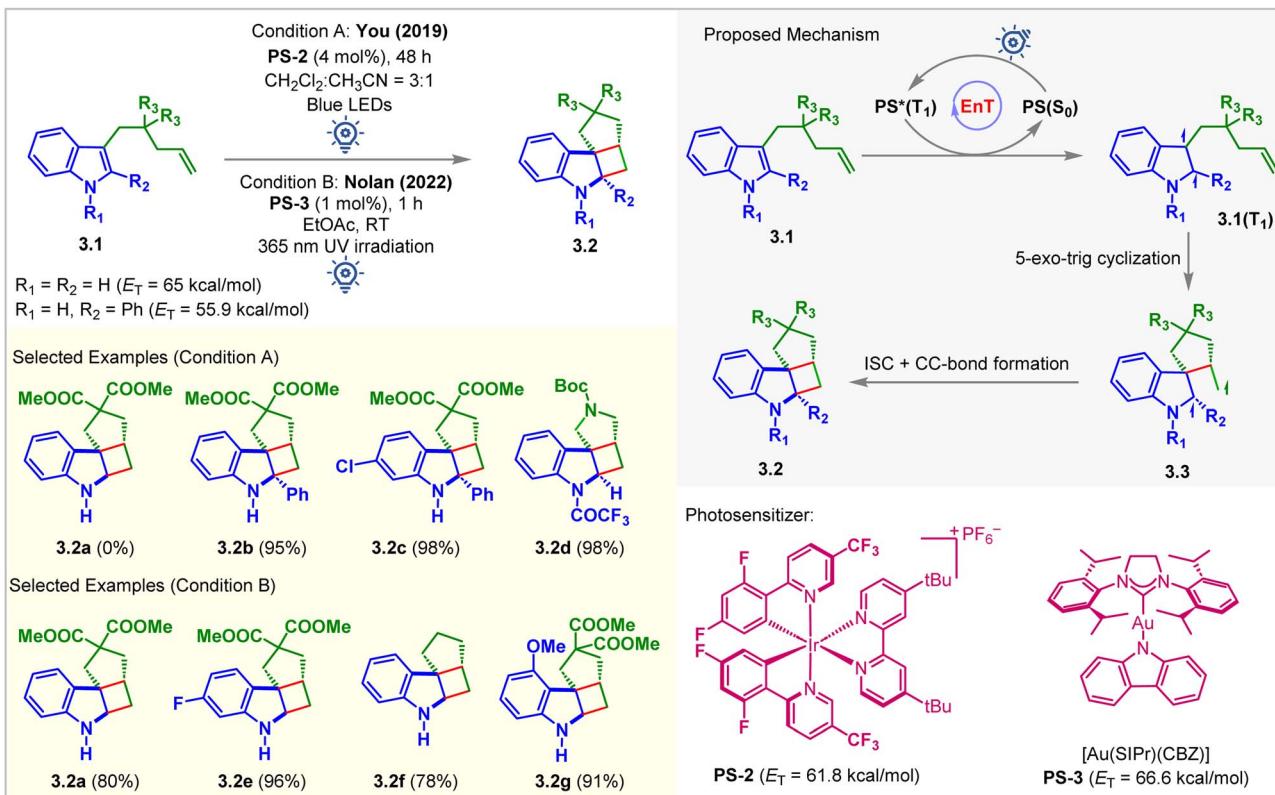
Fig. 3 Visible light-mediated EnT dearomative intramolecular [2π + 2π] cycloaddition of C3-alkene-tethered indole derivatives.

3.1(T₁) (Fig. 3). Subsequent 5-*exo*-trig cyclization forms diradical species **3.3**, which undergoes ISC followed by radical recombination to give the desired [2 + 2] cycloadduct **3.2**. Although this method tolerates substituted pendant olefin derivatives well, the cationic nature of iridium complexes and their low solubility limit the widespread application of this reaction. Nevertheless, a successful strategy was initiated for developing such highly strained molecules with contiguous quaternary centers. In 2022, Nolan *et al.* modified the above approach by using the carbene–metal–amido complex (Fig. 3, condition B).[50] The gold carbazolyl complex [Au(SIPr)(Cbz)] **PS-3** (E_T = 66.6 kcal mol⁻¹; uB3LYP/6-311+G(2d,p) level of DFT) acted as the sensitizer. It allowed the more facile intramolecular cycloaddition to occur in a shorter reaction time using greener solvents (MeOH, EtOAc, and i-PrOAc). However, 365 nm UV light irradiation was required. The authors successfully probed the cycloaddition of challenging unprotected indole, yielding a single diastereomer of the desired product **3.2a** in 80% yield. It was also confirmed that diester-substitution is unnecessary to form the cycloadduct **3.2f**. Indoles with electron-donating substituents were also well tolerated for this reaction forming **3.2g** with 91% yield. Quenching studies, light on/off experiments, cyclic voltammograms, and quantum yield determination provided evidence to support the mechanism *via* the EnT pathway.

In 2020, the Fu group fostered a novel and practical photocatalytic partial dearomative intramolecular [2 + 2] cycloaddition of indole derivatives **4.1** *via* hydrogen bond-influenced EnT (Fig. 4A).[51] Substrate **4.1** (E_T = 62.5 kcal mol⁻¹) has a relatively

higher E_T than **PS-2** (E_T = 61.8 kcal mol⁻¹) and **PS-4** (E_T = 55.2 kcal mol⁻¹), thus making the energy transfer step thermodynamically unfeasible. The reaction produced lower yields when **PS-2** and aprotic solvents, including CH_2Cl_2, MeCN, and DMF, were employed. Switching the nature of the solvent from aprotic to protic by introducing trifluoroethanol resulted in a dramatically improved yield of **4.2** up to 96%. The aggregation-induced and cooperatively enhanced H-bonds between the oxygen atom of the amide and trifluoroethanol were reasoned to be responsible for lowering the E_T of the substrate below that of the **PS-2**. In particular, when the electron-withdrawing group (COOMe, formyl, and phenyl) was substituted at the C2 or C3 position, an excellent, up to 97%, yield of **4.2d** was obtained.

In the same year, the You group disclosed the visible light-mediated EnT divergent partial dearomative cycloaddition of indole-tethered *O*-methyl oximes **4.3** (Fig. 4B).[52] The reaction was conducted in CH_2Cl_2 (0.01 M) in the presence of **PS-5**. The [2 + 2] cycloadduct **4.4b** was isolated as a single diastereomer in 97% yield. The presence of an EWG or an aryl group at the C2 position of indole achieved excellent results. However, the [2 + 2] cycloaddition of the 3-alkyl substituted indole moiety was interrupted after the first C–C bond formation. 1,5-hydrogen atom transfer (HAT) took place faster, delivering exocyclic C═C bonded products **4.5** (Fig. 4B). The computation studies (B3LYP/6-31G(d,p) level of DFT) suggested that formation of early stage [2 + 2] intramolecular dearomative cycloadducts **4.7** was kinetically controlled. When the reaction was allowed to continue, the consumption of **4.7** caused the regeneration of **4.6**, which
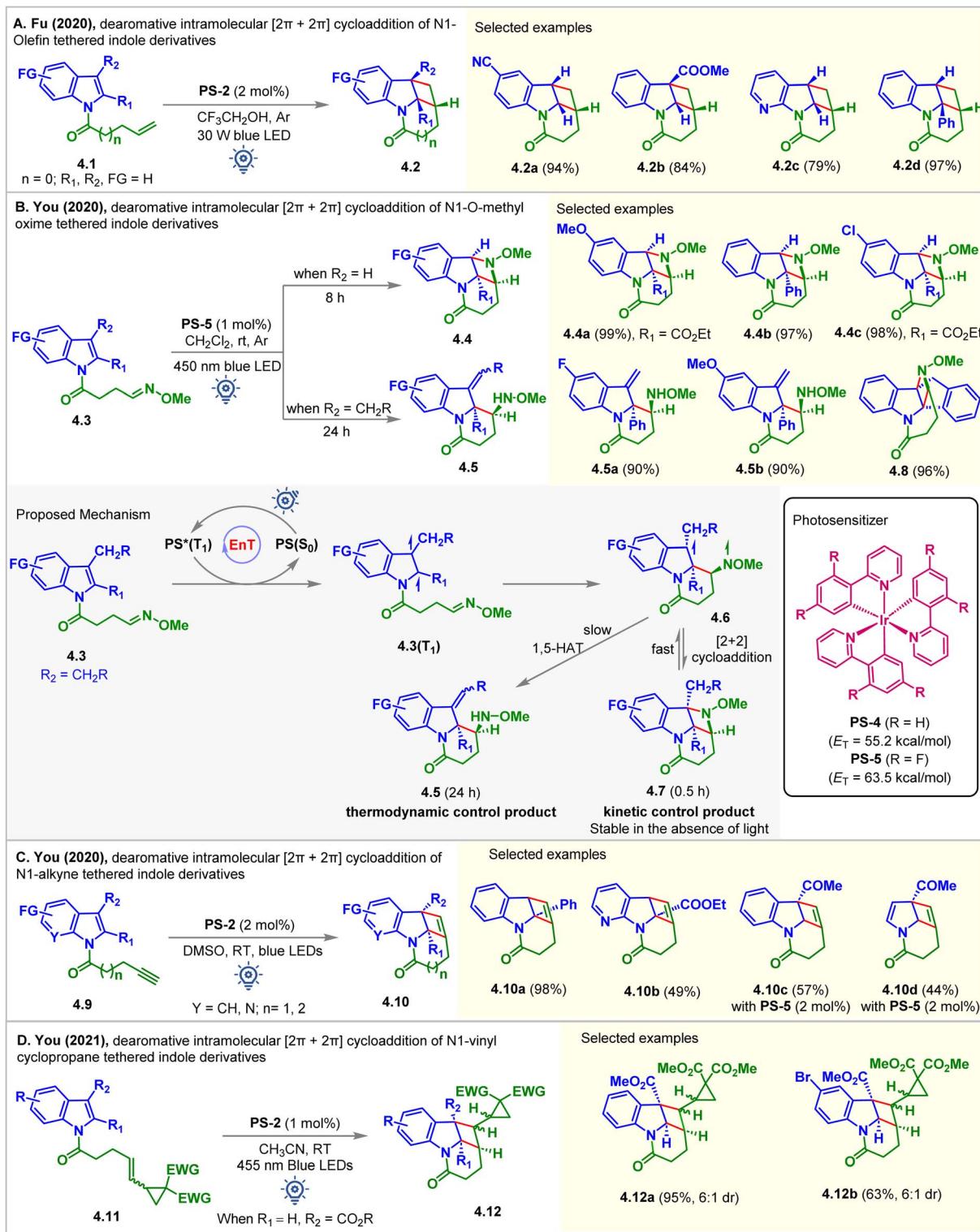
Fig. 4 Visible light mediated EnT dearomative intramolecular [2π + 2π] cycloaddition of (A) N1-olefin, (B) N1-*O*-methyl oxime, (C) N1-alkyne, and (D) N1-vinyl cyclopropane tethered indole derivatives.

then underwent 1,5-HAT to yield the thermodynamically controlled products **4.5**. Due to conformational restrictions preventing a 1,5-HAT process, an indene-fused substrate underwent dearomative [2 + 2] cycloaddition, providing product **4.8** in 96% yield.

At the same time, the You group also registered the intramolecular partial dearomative [2 + 2] cycloaddition of indole-tethered terminal alkynes **4.9** in the presence of **PS-2** under blue LED irradiation (Fig. 4C).[53] Tetracyclic cyclobutene-fused benzindolizidines **4.10** were formed in good to excellent yields

and >20 : 1 dr. An EWG (CO_2Et, CO_2Me) at the C2 position was necessary. Pyrrolo[2,3-b]pyridine derivative **4.10b** also underwent the reaction, albeit in moderate yields. However, due to the high E_T (up to 59.9 kcal mol^{-1}) for C3-EWG substituted substrates (**4.9**, R_1 = H, R_2 = CO_2Me, COMe, CN), **PS-2** furnishes the corresponding products in low yields (up to 57%). Interestingly, **PS-5** having higher E_T = 63.5 kcal mol^{-1} enabled their [2 + 2] cycloaddition to produce **4.10c** in moderate yields. Due to

the lack of resonance stabilization for the photo-generated unpaired electron, a pyrrole substrate underwent cycloaddition reactions to produce **4.10d** in a moderate 44% yield in the presence of **PS-5**.

Vinylcyclopropanes have demonstrated their applicability as an essential building block in several organic syntheses and frequent recurrence in many natural products.[54] The tendency to undergo easy ring-opening and capacity to generate
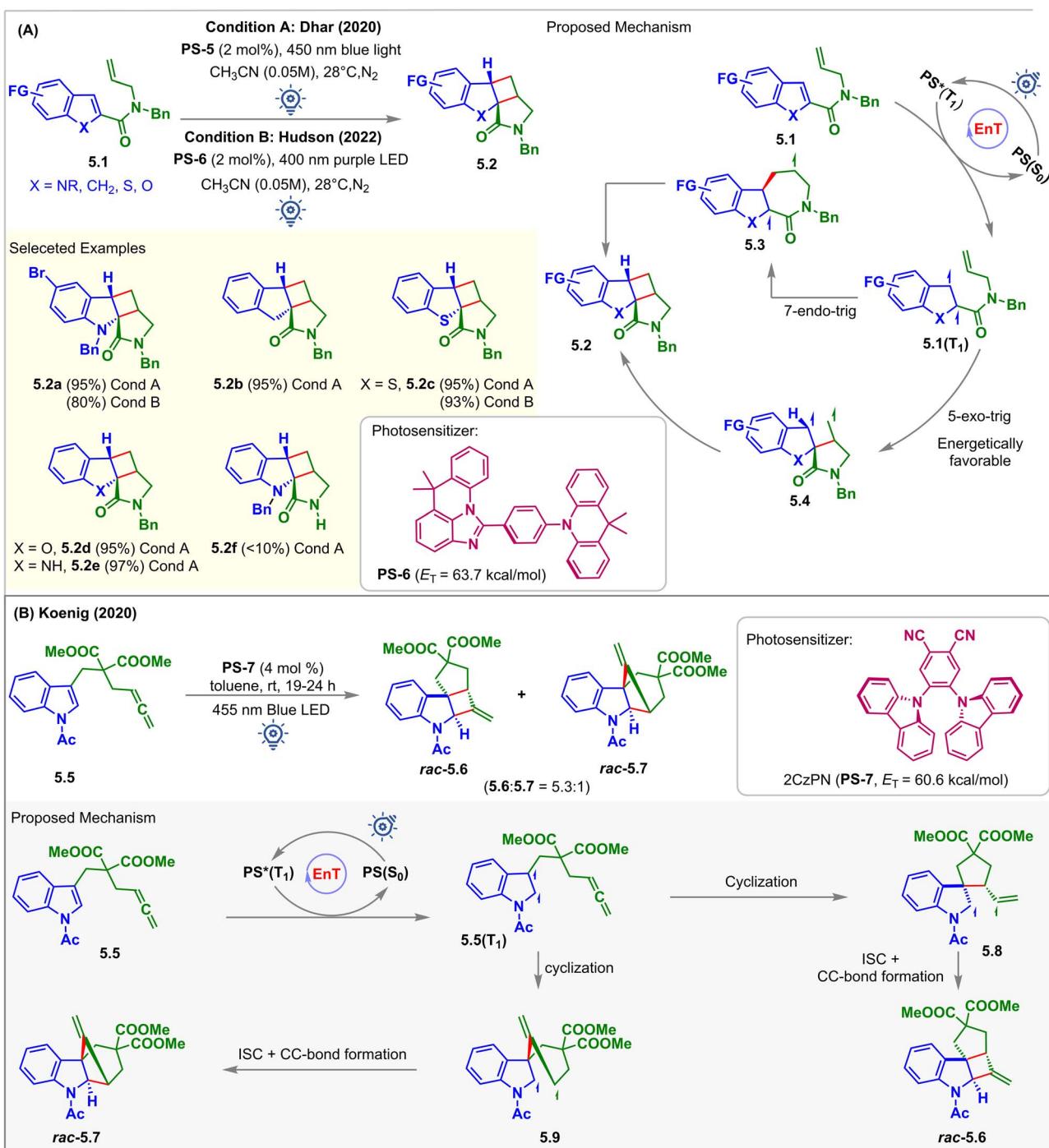
Fig. 5 Visible light mediated EnT dearomative intramolecular [2π + 2π] cycloaddition of (A) alkene tethered carboxamide of the indole/benzofuran/benzothiophene derivative, and (B) allene tethered indole derivatives.

diradicals make them a well-known reagent in radical clock experiments.[55] In 2021, You studied the partial dearomative cyclization of indoles and pyrroles with these units (Fig. 4D).[56] Upon irradiation with blue LEDs (24 W, λ_{max} = 455 nm), **PS-2** (1 mol%) catalyzed the dearomative [2 + 2] cycloaddition of C3-carboalkoxy substituted substrates **4.11** in MeCN. The cyclobutene-fused indolines **4.12** were produced in high yields with 6 : 1 dr. However, without a C3-carbomethoxy substituent, the same reaction produced [5 + 2] cycloadducts, not discussed in this manuscript. The authors attributed this alteration of the reaction pathway to the increase in steric bulk at the C3-position of the indole ring, which leads to alkene-generated diradical addition directly to the indole fragment in a facile [2 + 2] manner, thus circumventing the [5 + 2] cycloadduct formation.

In 2020, Dhar *et al.* reported the visible light-induced EnT partial dearomative intramolecular [2 + 2] cycloaddition reaction of C2-substituted heteroarenes **5.1** for the synthesis of cyclobutane–pyrrolidinone-fused tetracyclic scaffolds **5.2** (Fig. 5A, condition A).[57] There are two potential routes of ring closure leading to the formation of the product: (a) 5-*exo*-trig; and (b) 7-*endo*-trig, as demonstrated in the proposed mechanism (Fig. 5A). A computation study (B3LYP/6-311+G(2d,p) level of DFT) revealed that the former pathway was energetically more favorable than the latter. Tethering of olefin in the carboxamide substituent at the C2 position lowers the E_T to <60 kcal mol^{-1} when compared to the olefin tethered at the C3 position of carboxamide, which has E_T > 60 kcal mol^{-1}. This was due to the enhanced stability *via* extended conjugation of the diradical intermediates **5.1(T$_1$)**, which eliminated the requirement for the phenyl and ester group at the C2 position, as shown in Fig. 3 (condition A). The scope of the substrates went well beyond the indole-based moiety where C2 substituted indenes (**5.1**, X = CH$_2$), benzothiophenes (**5.1**, X = S), and benzofurans (**5.1**, X = O) with E_Ts less than 60 kcal mol^{-1} were also capable of undergoing intramolecular dearomative cycloaddition with excellent 93–95% yield to produce **5.2b**, **5.2c**, and **5.2d**, respectively. With the irradiation of the photosensitizer (**PS-5**), substrates **5.1** undergo 57% conversion in 24 h, and for the complete transformation, 48 h was required. With 400 nm purple light, the reaction was accelerated, and **5.1** was fully reacted within 18–24 h. However, for the 6-bromo-functionalized indole derivative, a 5% proto-debromination side product was observed in the presence of higher energy 400 nm light. An excellent yield of 97% was also observed for cycloadduct **5.2e** with an unprotected indole. However, only small quantities of cycloadduct **5.2f** were observed for substrates bearing an unprotected carboxamide group.

In 2022, Hudson *et al.* demonstrated imidazoacridine-based thermally activated delayed fluorescence (TADF) material (ACR-IMAC, **PS-6**) to be an affordable, highly effective organic alternative to the commonly used iridium-based PSs for visible light EnT catalysis (Fig. 5A, condition B).[58] The twisted donor–acceptor architecture of these materials accelerates rapid ISC and widens the HOMO–LUMO energy gap, thus minimizing electron transfer phenomena. Besides, high E_Ts (63.7 kcal mol^{-1}), extended excited state lifetimes (64 μs), and poor oxidizing properties make them effective PSs in visible light-

mediated EnT reactions. It has been demonstrated that the TADF material **PS-6** completely converts **5.1** to cycloadducts **5.2** under purple LED irradiation. However, the efficiency dropped to a yield of 51% when exposed to blue light. The derivatives of benzo-thiophene, chromene, and indene also experience a similar dearomative [2 + 2] cycloaddition with excellent yield and high diastereocontrol (dr > 99 : 1). However, the cycloaddition of indole with an alkyne did not proceed successfully.

In 2020, Koenig investigated the potential of low-cost 2CzPN (**PS-7**, E_T = 60.6 kcal mol^{-1}) as a **PS** over well-known iridium-catalysts to carry out the partial dearomative cycloaddition of allene-tethered indoles **5.5** in the presence of blue LEDs (Fig. 5B).[59] Ohkuma previously attempted the same reaction using a high catalyst loading of 3′,4′-dimethoxyacetophenone (50 mol%) as the **PS**. However, this involved irradiation from a high-energy mercury lamp through Pyrex glass.[60] In this report, the desired *cis*-fused methylenecyclobutane-containing products were obtained in 80% yields with high stereoselectivity along with a trace amount of undesired alkyne product *via* 1,5-HAT. Also, incorporating –OMe and –COOMe groups at the C5 position reduced the reaction rates, producing undesirable deacylated or photo-Fries rearranged side products. However, the employment of **PS-7** by Koenig *et al.* overcame the difficulties mentioned above. With the irradiation of **PS-7** in the presence of a 455 nm light source, substrates **5.5** produced a mixture of *rac*-**5.6** and *rac*-**5.7** in a 5.3 : 1 ratio in toluene. The solubility of uncharged **PS-7** in toluene allows its easy recovery and reuse over several cycles. Non-polar solvents inhibited electron transfer from indole derivatives **5.5** to **PS-7**, indicating EnT to be the operative mechanistic pathway. The presence of two ester groups facilitates ring closure *via* the Thrope–Ingold effect.

In 2022, Bach accessed the low-lying triplet states of aryl iminium ions **6.1** *via* EnT (Fig. 6).[61] Olefin-tethered aryl iminium ions **6.1** produced the [2 + 2] cycloadducts **6.2** in the presence of 2.5 mol% thioxanthone (TXT, **PS-8**, E_T = 63.1 kcal mol^{-1}) under 420 nm blue light irradiation for 18 h. Cycloadducts **6.2** undergo iminium ion-triggered rearrangement to produce cyclized products **6.3**. The rearranged products **6.4** were isolated after treating the reaction mixture with aq. NaOH. Carbon-tethered olefinic and alkyne-tethered aryl iminium ions were found to be unreactive, proving the necessity of the oxygen substituent at the 2-position of iminium ions **6.1** to carry out the cycloaddition. Notably, under standard conditions, methoxy-substituted arenes and those with a substituent at the 5-position failed to give expected products which the authors attributed to inaccessibility of the respective triplet states due to change in electronic properties.

2.2. Intermolecular [2π + 2π] *ortho*-cycloaddition

Due to entropic challenges, the intermolecular [2 + 2] cycloaddition reactions are more demanding than the intramolecular ones. Besides, the EnT-generated excited state of the substrate must be long-lived to be intercepted by the coupling partner. In 2018, Meggers *et al.* reported the first visible-light-induced intermolecular dearomative [2 + 2] cycloaddition of 2-*N*-
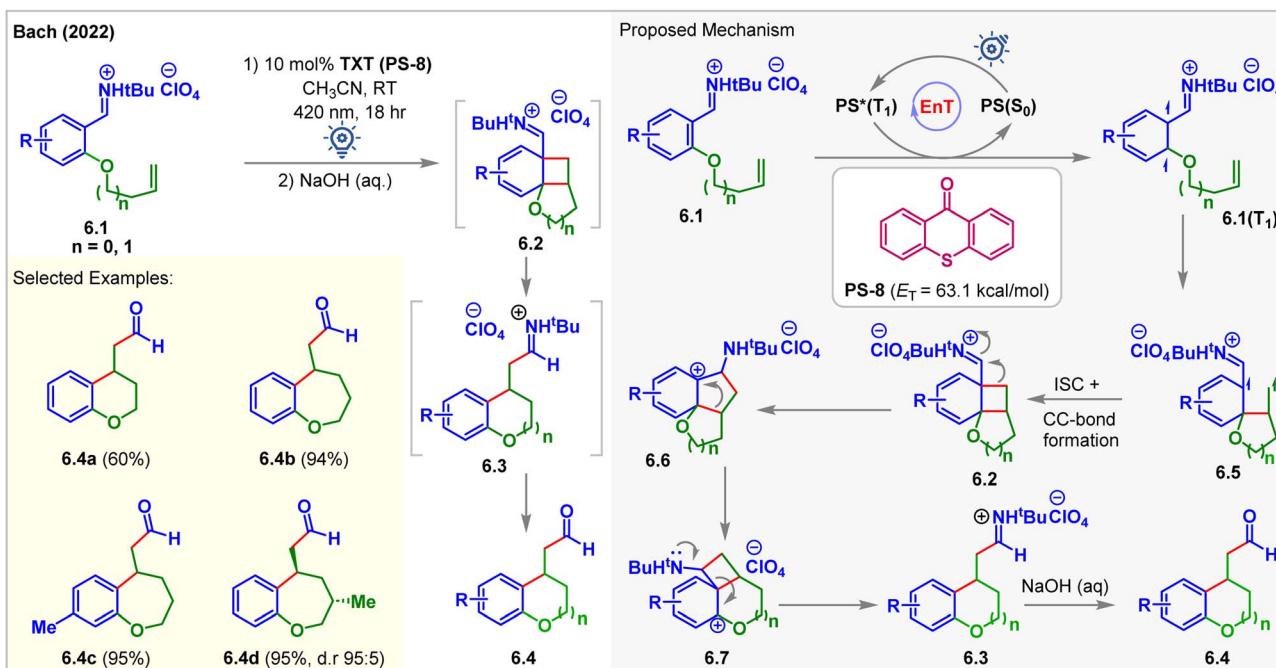
Fig. 6 Visible light-mediated EnT dearomative intramolecular [2π + 2π] cycloaddition of an olefin tethered aryl-iminium ion.

acylpyrazole-substituted benzofurans **7.1** with styrenes **7.2** using a chiral-at-rhodium complex **PS-9** (2 mol%) as the catalyst (Fig. 7).[62] The cycloadducts **7.3** were isolated in high yields with up to 98% ee on exposure to blue LED irradiation with **PS-9** for 18 h. The reaction also yielded minor diastereomers **7.4** and regioisomers **7.5**. Due to the lability of the *N*-acyl pyrazole moiety, the initially formed cycloadduct was treated with methanol in the presence of a base to isolate methyl ester **7.3** as the product. The diastereo- and regioisomeric ratios depended on the nature of substituents on styrenes. The reaction with parent styrene produced **7.3a** in 78% yield with 98% ee, 6.2 : 1 dr, and 5.3 : 1 rr. Computation studies (B3LYP/6-31G(d,p) level of DFT) supported this observation. The (*Z*)-β-methyl styrene produced **7.3b** in 90% yield with 97% ee and very high (>20 : 1) dr and (>20 : 1) rr when irradiated at −30 °C. The dr was found to be temperature dependent, as the same reaction produced a poor 1.8 : 1 dr under room temperature conditions. This observation was consistent with the formation of a biradical intermediate where temperature plays a crucial role in the rotation of the C–C single bond, *vide infra*. When (*E*)-β-methyl styrene took part in the reaction, the opposite diastereomer **7.4a** was formed as the major product (>20 : 1 dr, >20 : 1 rr) in 90% yield with 99% ee. The presence of electron-donating, electron-withdrawing, and sterically hindered groups at the *meta* and *para* positions of the styrene aromatic ring was well tolerated while safeguarding the dr and rr. As an exception, an *ortho*-substituted styrene gave lower rr and dr of the product **7.3c**. Interestingly, a chiral-at-iridium analog of **PS-9** showed no conversion at all. Mechanistically, the substrate **7.1** was initially associated with **PS-9** to form the [**7.1-Rh**] complex, as shown in Fig. 7. After the EnT from excited photosensitizer **PS*(T₁)**, the substrate-sensitizer complex [**7.1-Rh**] got excited to its triplet

state [**7.1-Rh**](**T₁**). The latter then reacted with **7.2b** to form the biradical intermediate **7.6**, and the stability of the 1,4-benzyl radical **7.6** determined the regioselectivity. Then, ISC, followed by C–C bond formation, generated the **7.7** complex, followed by the ligand exchange between **7.1** and **7.7** to liberate the product **7.8** and close the catalytic cycle. As a post-synthetic transformation, the methanolysis of **7.8** afforded **7.3b** in 90% yield and 97% ee.

In 2021, the Oderinde group employed a substrate-based screening approach to examine indole derivatives **8.1a–8.1g** for partial dearomative intermolecular [2 + 2] cycloaddition reaction (Fig. 8).[63] Thermodynamically, accessing the indole triplet-states (E_T = 68–70 kcal mol⁻¹) from most PSs (E_T = 40–64 kcal mol⁻¹) is improbable which is also supported by the B3LYP/6-311+G(2d,p) level of DFT calculations. Installing an EWG at the C2 position lowers the E_T of the indole moiety and should ideally make the desired cycloadditions more facile. However, with the irradiation of [Ir(dF(Me)ppy₂)dtbbpy]PF₆ (**PS-10**, E_T = 62.9 kcal mol⁻¹) under 450 nm blue LEDs, the indole derivatives **8.1d–8.1g** did not undergo intermolecular [2 + 2] cycloadditions with vinylsilane **8.2**, despite having a lower E_Ts than **PS-10**. It was hypothesized that the excited triplet diradical species derived from **8.1d–8.1g** were too short-lived to undergo intermolecular cycloaddition reactions. While a 76% head-to-head homo-dimer product along with 24% minor cycloadduct **8.3a** was produced from **8.1a**, the indole derivative **8.1b** experienced cycloadditions with vinylsilane **8.2** to produce cycloadduct **8.3b** in 50% yield, along with head-to-tail homo-dimers **8.4**. Notably, *N*-Boc-indole **8.1c** reacted with vinylsilane **8.2** to produce the cycloadduct **8.3c** in an excellent 95% yield, >20 : 1 rr, and 16 : 1 dr. Without vinylsilane, **8.1c** underwent homo-dimerization to produce **8.4c** in 98% isolated yield, implying
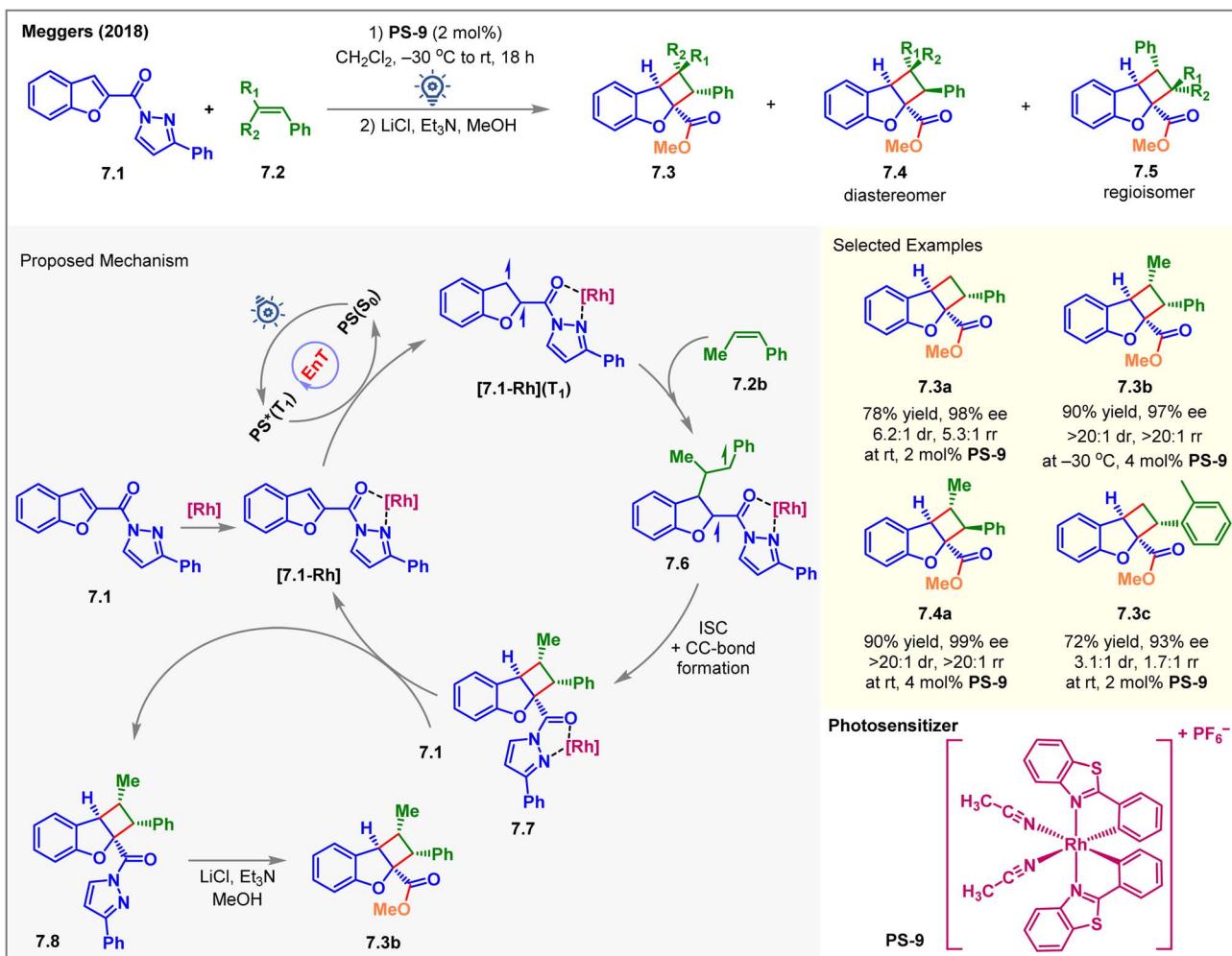
Fig. 7 Visible light-mediated EnT asymmetric dearomative intermolecular [2π + 2π] cycloaddition of 2-N-acylpyrazole-substituted benzofuran derivatives with a chiral-at-rhodium photosensitizer.

that productive cross-cycloaddition occurred significantly faster than homodimerization. Additionally, the reactions could also be carried out in higher yields using purple LEDs (=400 nm) in the presence of poorly oxidizing sensitized **PS-5** (Ir(III)*/Ir(II) =

0.36 V vs. SCE). While exploring the alkene scope, the authors observed that bulky substituents on the alkenes enhanced the dr. Modest yields were obtained while extending the methodology for the reactions with various alkynes. Homodimerized
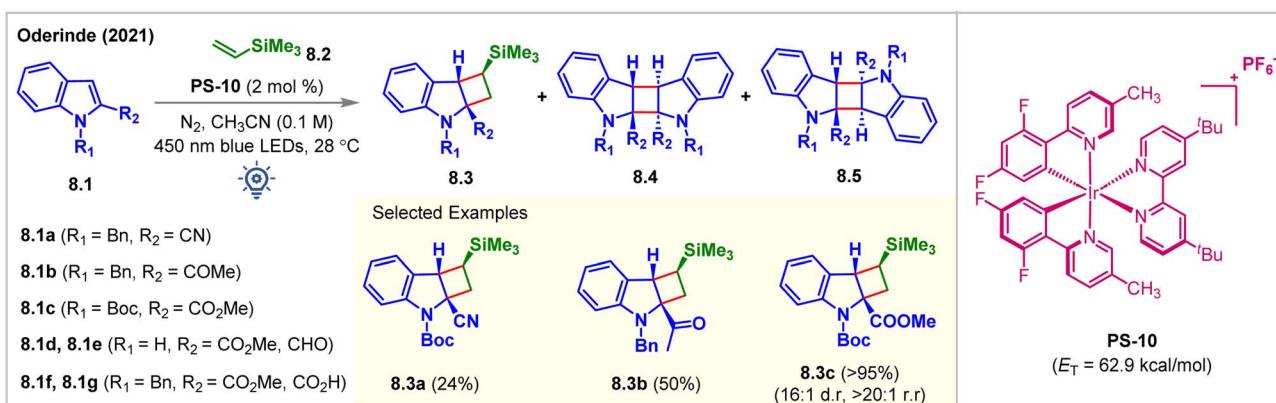

Fig. 8 Visible light mediated EnT dearomative intermolecular [2π + 2π] cycloaddition of various indole derivatives with vinylsilane.

products are the major side products. It is implied that the cross-cycloaddition reaction with alkynes was less efficient than that with alkenes.

2.3. Intermolecular [2π + 2σ] *ortho*-cycloaddition

Rigid saturated cyclic scaffolds with complex three-dimensionality, such as bicylo[1.1.0]butanes (BCBs), have become increasingly relevant bioisosteres and valuable medicinal chemistry motifs.[64,65] The distortions of the ring in BCBs forced them to flip the ring between different configurations at high temperatures.[66] They have different bond angles distorting from a planar conformation with high *p*-character (96%) in the central C–C σ-bond (Fig. 9A). This central C–C σ-bond has been shown to interact with a wide variety of electrophiles and nucleophiles, in processes ranging across a variety of thermal[67] and photochemical cycloadditions (Fig. 9A).[68] Recent studies showed that the BCBs could undergo [2π + 2σ] cycloadditions with alkenes by cleaving this bridge σ-bond.[69–72] Glorius and Houk utilized this strategy for the intermolecular dearomative [2π + 2σ] cycloaddition of quinolines **9.1** with BCBs **9.2** (Fig. 9B).[73] **PS-2** (2 mol%) catalyzed the reaction with the aid of a Lewis acid Sc(OTf)₃ (0.5 equiv.). The reaction produced C(sp³)-rich bicyclo[2.1.1]hexanes (BCHs, **9.3**) in CH₂Cl₂ under 450 nm blue LED irradiation of **PS-2** for 16 h at room temperature. The

BCH **9.3a** was isolated from 7-methoxyquinoline **9.1a** in 89% yield. It was observed that both the reaction partners could not absorb 450 nm light. However, in the presence of Sc(OTf)₃, a bathochromic absorbance shift for both substrates was noticed. The product **9.3a** was formed in 43% yield even in the absence of **PS-2** with Sc(OTf)₃ (1 equiv.) *via* direct excitation. Sulfone-substituted BCB also underwent the [2π + 2σ] cycloaddition reaction to produce **9.3b** in 67% yield. 1,3-Disubstituted BCBs also participated, and the product **9.3f** bearing a quaternary carbon center at the bridge-head position was formed without Lewis acid. 4-Substituted quinolines were also tolerated. However, a 7-methoxy substituent was necessary. Stern–Volmer quenching studies revealed significant quenching of the excited **PS** by 7-methoxy quinoline **9.1a**. The DFT study at the UωB97XD/def2TZVPP/SMD (solvent = DCM)//UM06-2X/def2SVP level of theory showed that the Lewis acid Sc(OTf)₃ lowers the E_T of **9.1a** (E_T = 62.6 kcal mol⁻¹) by 10.5 kcal mol⁻¹ such that the EnT from **PS-2** (E_T = 61.8 kcal mol⁻¹) to the quinoline–scandium adduct **9.4** is highly exergonic. The resulting **9.4(T₁)** biradical species attacked the BCBs **9.2**. The ISC is followed by C–C bond formation to give the desired [2π + 2σ] cycloadduct. The authors also proposed an alternative biphotonic radical chain propagation mechanism where the radical cations **9.7** were hypothesized to be formed *via* the SET mechanism in two different reaction pathways. The
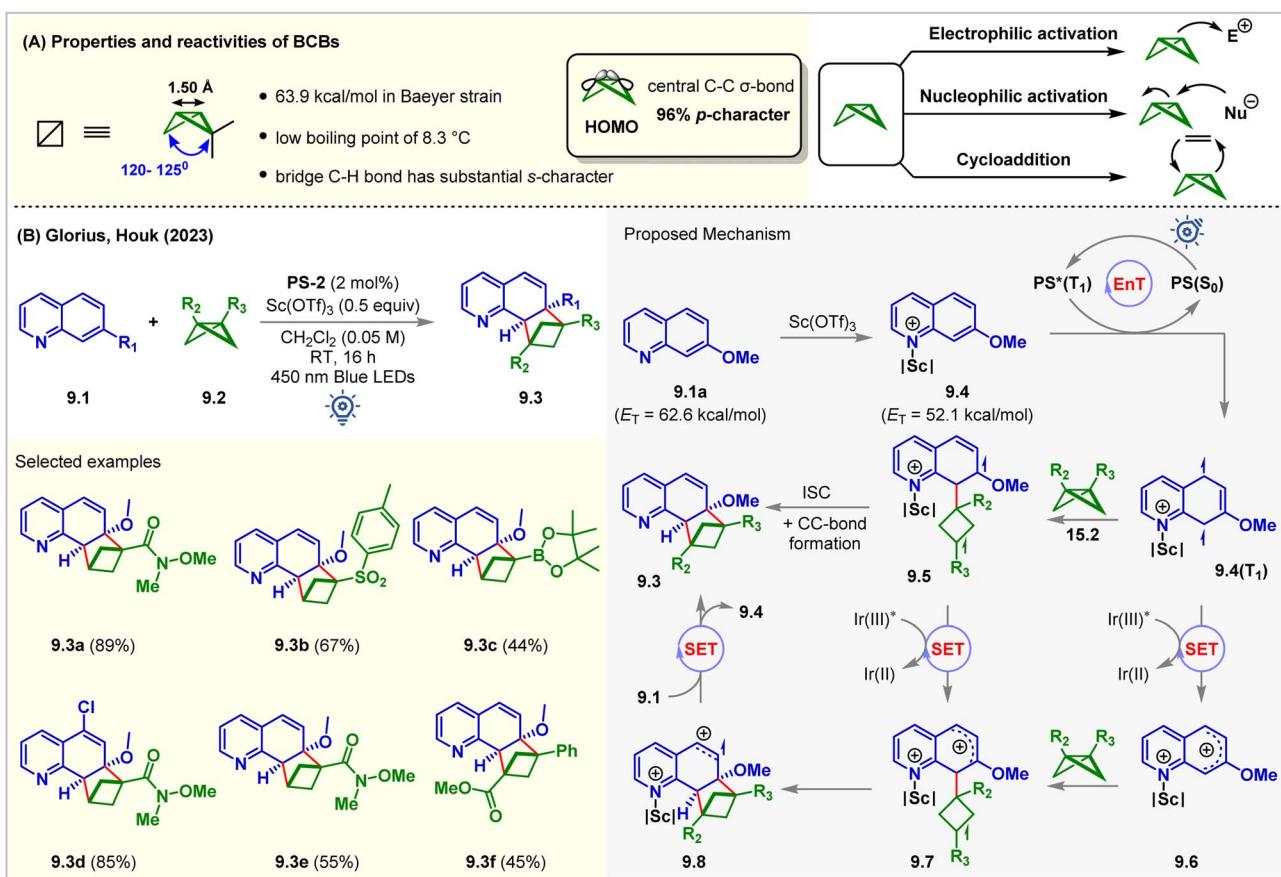
Fig. 9 (A) Properties and reactivity of BCBs and (B) visible light mediated EnT dearomative intermolecular [2π + 2σ] cycloaddition of 7-methoxy quinolines with BCBs.

intermolecular cyclization of **9.7** forms another radical cation, **9.8**, which then transforms into product **9.3** after undergoing a SET from quinolines **9.1**, propagating the chain. Recently, Glorius reported the insertion of BCB to the thiophene moiety towards dearomative ring expansion *via* a photocatalyzed SET mechanism.[74]

3. Dearomative [4π + 2π] *para*-cycloaddition

The Diels–Alder reaction represents one of the powerful methods for six-membered ring synthesis.[75–79] Electron-rich dienes and electron-deficient dienophile partners or *vice versa* assure high yields and reactivity explained by using the frontier molecular orbital (Fig. 10A).[80] In 1989, Hamrock and Sheridan reported selective [4 + 2] or *para*-cycloaddition of benzene with 4-methyl-1,2,4-triazoline-3,5-dione (MTAD) under visible light irradiation at −60 °C (Fig. 10B).[81] Low-temperature requirement was necessary for generating an arene–alkene cycloadduct as retro-cycloaddition happens at a temperature greater than −10 °C. The cycloaddition mechanism was not appropriately understood, indicating that either electron transfer or charge transfer or both become plausible pathways of cycloaddition between photo-activated MTAD and benzene. Subsequently, *para*-cycloaddition appeared in the literature through the work of Wilzbach and Kaplan,[13] Gilbert and Taylor,[82] DÖpp,[83] Bochet,[84] and others under high energy UV irradiation. Recently, Sarlah studied arene-MTAD cycloaddition in detail and coupled the photocycloaddition reaction with transition metal-catalyzed
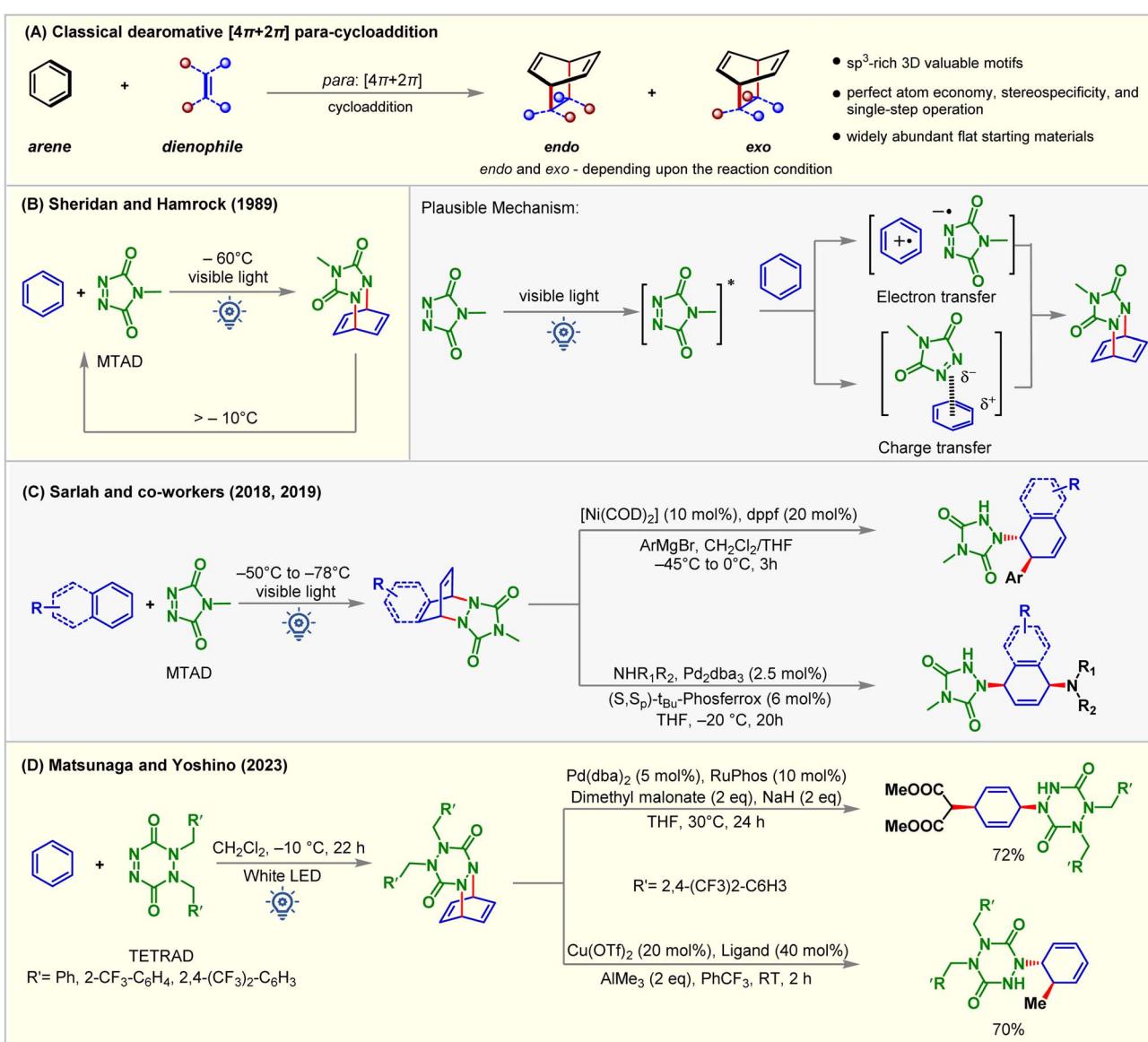

Fig. 10 (A) Classical [4 + 2] *para*-cycloaddition reaction, (B) *para* [4 + 2] cycloaddition of benzene with MTAD under visible light irradiation, (C) transition metal-catalyzed amino-functionalization of simple arenes, and (D) [4 + 2] *para*-cycloaddition of TETRAD and benzene and further applications.

amino-functionalization (Fig. 10C),[85–87] and dihydoxylation reactions.[88] It was found that MTAD got excited for the cyclo-addition process. The application of dearomatization has become a revolutionary method in addressing the significant challenges synthetic chemists face. The isolation and detailed characterization of MTAD-benzene cycloadducts were difficult due to their lower thermodynamic stability. This becomes a significant drawback that restricts understanding reactivity and further applications. Recently, Matsunaga and Yoshino[89] demonstrated that the [4 + 2] cycloadduct of 1,2-dihydro-1,2,4,5-tetrazine-3,6-diones (TETRADs) and benzene could be isolated by the chromatographic technique and characterized by NMR and XRD (Fig. 10D). Interestingly, the further transformation of the TETRAD-benzene cycloadduct occurs above room temperature.

When electronically mismatching cycloaddition partners are used, the requirement of high temperature, pressure, and UV irradiation strongly limits their widespread application in chemical and pharmaceutical industries.[90] Electronically mismatched cycloaddition can be enabled by photoinduced SET or chemical oxidation using stoichiometric oxidants.[91] Since the high-energy UV-light and stoichiometric redox reagents negatively impacted the sustainability of the reaction, the visible-light-induced [4 + 2] cycloaddition reaction using catalytic PSs is a promising alternative.[89] As discussed earlier, the reluctance of arenes to lose aromaticity is a crucial challenge that needs to be overcome. It is relatively easy for hetero-aromatic compounds and phenol derivatives with less aroma-ticity to undergo dearomative transformations, whereas it is highly challenging for benzene derivatives due to their enhanced aromaticity.[92] Dearomative [4 + 2] *para*-cycloaddition employing light mainly focuses on sensitizing alkene partners instead of the arene.[93] Visible-light-EnT-mediated direct sensi-tization of the arene derivatives is still developing. The main focus of the next section is to summarize the recent develop-ment of EnT dearomative [4 + 2] cycloaddition reactions under the influence of visible light. Both arene and arenophile

Fig. 11 Visible light mediated EnT dearomative intramolecular [4π + 2π] cycloaddition of (A) pyridine tethered *N*-cinnamoyl picolinamide derivatives using [Ir-F]@polymer PS-11 as a photosensitizer and (B) arene tethered *N*-cinnamoyl picolinamide derivatives.
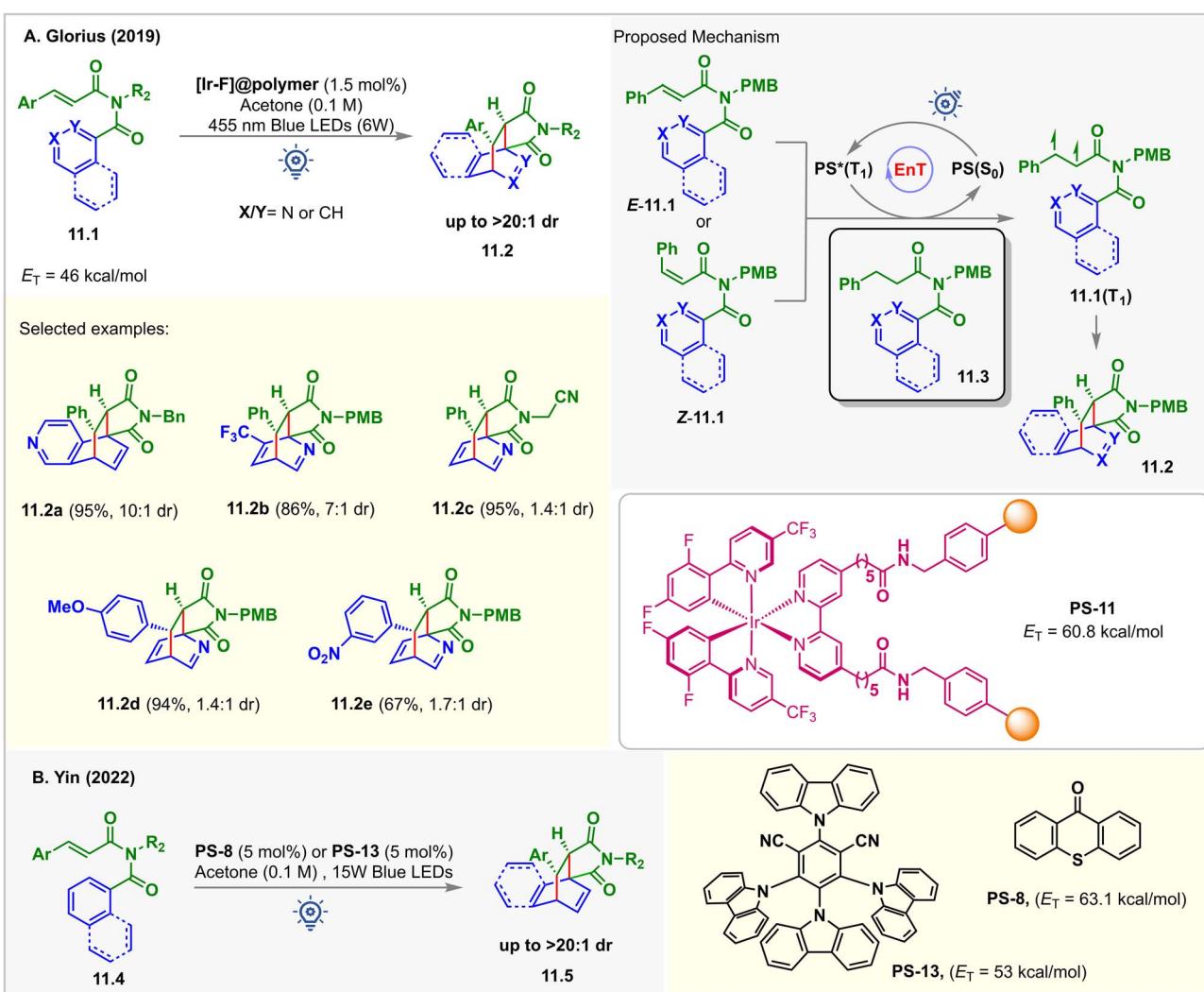
excitation are discussed depending on the accessibility of their triplet states.

3.1. Intramolecular [4π +2π] *para*-cycloadditions

Pyridine derivatives are incompatible with photocatalytic reactions due to their redox inactivity and high $E_T > 70$ kcal mol^{-1}, making it challenging for them to undergo SET and EnT processes.[94] However, the triplet states of the alkenes could be accessed to enable their cycloaddition with pyridines. In 2019, Glorius reported an intramolecular dearomative [4 + 2] cycloaddition of *N*-cinnamoyl picolinamide derivatives **11.1** *via* EnT catalysis (Fig. 11).[95] A polymer immobilized [Ir-F]@polymer **PS-11** (1.5 mol%, $E_T = 60.8$ kcal mol^{-1}) was used as a catalyst. The EnT from photoexcited **PS-11** to the pyridine substrates **11.1** ($E_T = 46$ kcal mol^{-1}) was thermodynamically feasible, which is also supported by computational studies at the (U)CAM-B3LYP/def2-TZVPP/CPCM (MeCN) level of theory. The [4 + 2] cycloadducts **11.2** were isolated in excellent yield when irradiated with 455 nm blue 6 W LEDs in acetone. Interestingly, the cycloaddition was highly tolerant to changes in reaction conditions. While optimizing the reaction conditions, it was observed that diverse solvents, including CH$_2$Cl$_2$, THF, CH$_3$CN, and even water, could be used without affecting the yield of the products. 0.75 mol% of **PS-11** loading also reproduced the same outcome. In addition, isoquinoline, naphthyl, and phenyl derivatives also underwent the dearomatization reaction smoothly with excellent dr under the same conditions. Ease of separation from the reaction mixture and a high degree of recyclability brings added benefits for **PS-11**. The catalyst was recyclized up to 10 times

without any drop in its efficiency. Kinetic monitoring of the reaction showed the formation of only [4 + 2] cycloadducts **11.2**. *E* to *Z* isomerization of the substrate was also noticed. This implied that **E-11.1** and **Z-11.1** converted to the same 1,2-biradical intermediates **11.1(T$_1$)** that produced **11.2**. The selectivity for the [4 + 2] cycloadduct over [2 + 2] and [3 + 2] is justified by the thermodynamic stability of the products. Stern–Volmer analysis revealed the quenching of excited PS by *N*-cinnamoyl picolinamides **11.1**, whereas no quenching was observed for the reduced substrates **11.3**. This inferred that the EnT took place from the PS to the styrene pendant of the substrate to form 1,2-biradical intermediates **11.1(T$_1$)** that then produced **11.2** *via* CC-bond formation, ISC, and the radical coupling sequence.

In 2022, the Yin group demonstrated a similar dearomative intermolecular [4 + 2] *para*-cycloaddition of arene-tethered *N*-cinnamoyl picolinamide derivatives **11.4** (Fig. 11B).[96] **PS-8** (1 mol%) or **PS-13** (5 mol%) catalyzed the reaction in acetone solvent under irradiation of 15 W purple or blue LEDs. A series of bridged bicyclo scaffolds **11.5** were prepared with excellent diastereoselectivity (>20 : 1 dr).

In 2021, the You group developed a double dearomative cycloaddition of indole derivatives bearing a pendant 1-naphthyl ring **12.1** (Fig. 12).[97] Bridged cyclic-indoline **12.2a** was produced in 97% isolated yield with >20 : 1 dr in the presence of 1 mol% of **PS-5** in CH$_2$Cl$_2$ at rt under the irradiation of blue LEDs for 5 h. With the increasing steric bulk at the C2- and C3-positions of the indole moiety, a longer time (up to 3 days) was required to reach high yields. Also, indoles with both electron-donating and withdrawing groups reacted smoothly to
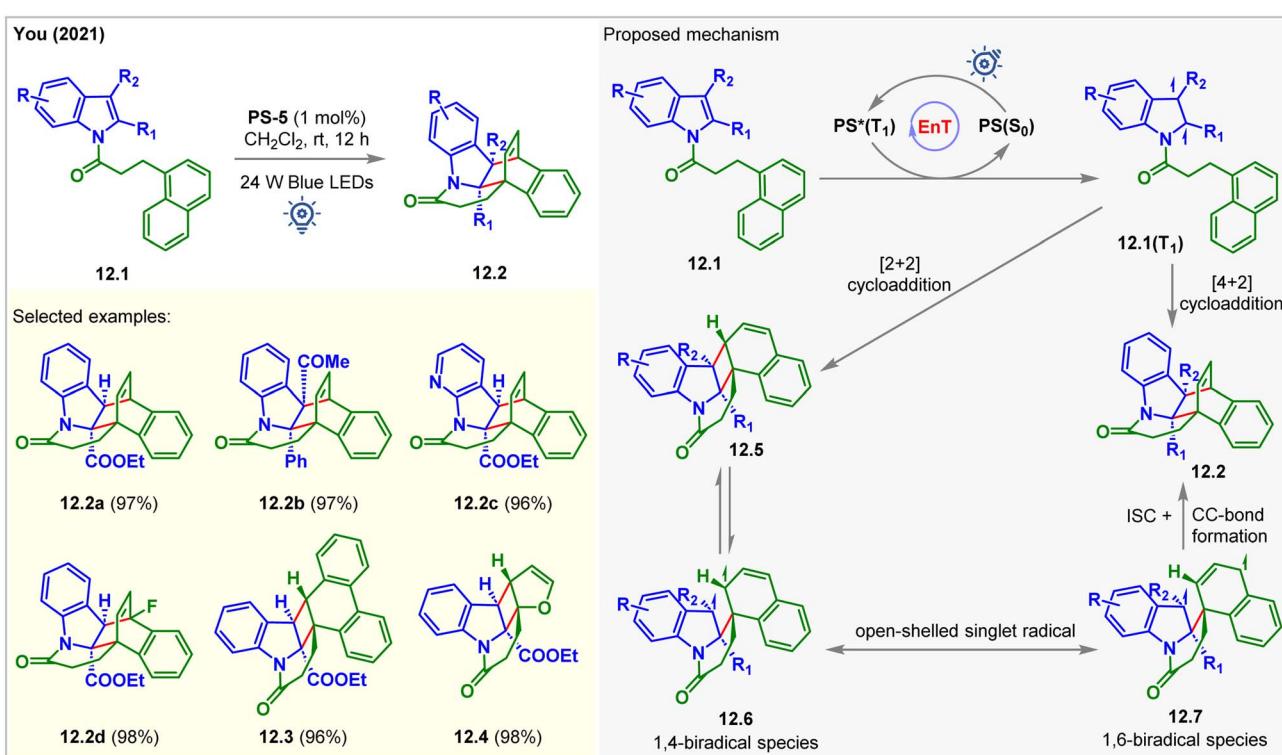

Fig. 12 Visible light mediated EnT double dearomative intramolecular [4π + 2π] cycloaddition of an N1-naphthalene tethered indole derivative.

produce excellent 93–98% yields. The pendant 2-naphthyl ring and 9-anthracene rings led to a [4 + 2] cycloaddition product. In comparison, 9-phenanthrene gave [2 + 2] cycloadduct **12.3** with 96% yield. The [2 + 2] cycloaddition products were also observed for pendant 2-furyl (**12.4**), 3-furyl, and 2-benzofuryl derivates of indole. The kinetic analysis of the reaction revealed that dearomative [2 + 2] cycloadducts **12.5** were produced initially. As the reaction progressed, **12.5** were consumed, and **12.2** were formed. During this process, **12.5** is in equilibrium with the 1,4-biradical **12.6**, which is itself removed from equilibrium by radial recombination from its resonance form **12.7**. The desired double dearomative [4 + 2] cycloadducts **12.2** were formed after radical addition.

Recently, the Maestri group photosensitized allenamides for their intramolecular dearomative [4 + 2] cycloaddition with tethered arenes (Fig. 13).[98] **PS-4** was used as the catalyst under visible light irradiation in DMF. The author found that naphthyl derivatives **13.1** reacted twice faster than the derivative of simple arenes **13.2**. The products **13.3** and **13.4** were isolated in 18–99% yields in 16–96 h. Allenamides having naphthyl side

arms **13.1** were found to quench the excited **PS-4** at a higher rate $K_{SV} = 404$ M^{-1}. The formation of [4 + 2] cycloadducts **13.3** from **13.1** could possibly occur via two reaction pathways involving two different biradical intermediates, **13.5** and **13.6**. The spin density of the triplet biradical intermediates **13.5** were found to be localized on the allenyl fragment. It was suggested that the intramolecular attack of the excited allene onto the naphthyl moiety of **13.5** proceeds via a low-energy transition state to generate spiro triplet biradical intermediates **13.7**. On the other hand, the spin density of **13.6** was localized on the naphthyl moiety. Since the formation of the intermediate **13.7** from **13.6** involved a high-energy transition state, this pathway was considered to be less favorable. However, in the case of allenamide containing a phenyl arm **13.2**, the involvement of a more energy-costly TS and less stable intermediate **13.9** was responsible for the slower reaction. Mechanistically, the EnT-generated triplet vinyl radical intermediates **13.8** attacked the benzyl arm, broke the aromaticity, and produced the triplet biradical intermediates **13.9**. The ISC to the singlet intermediates **13.10**, followed by CC-bond formation, yields the [4 + 2]
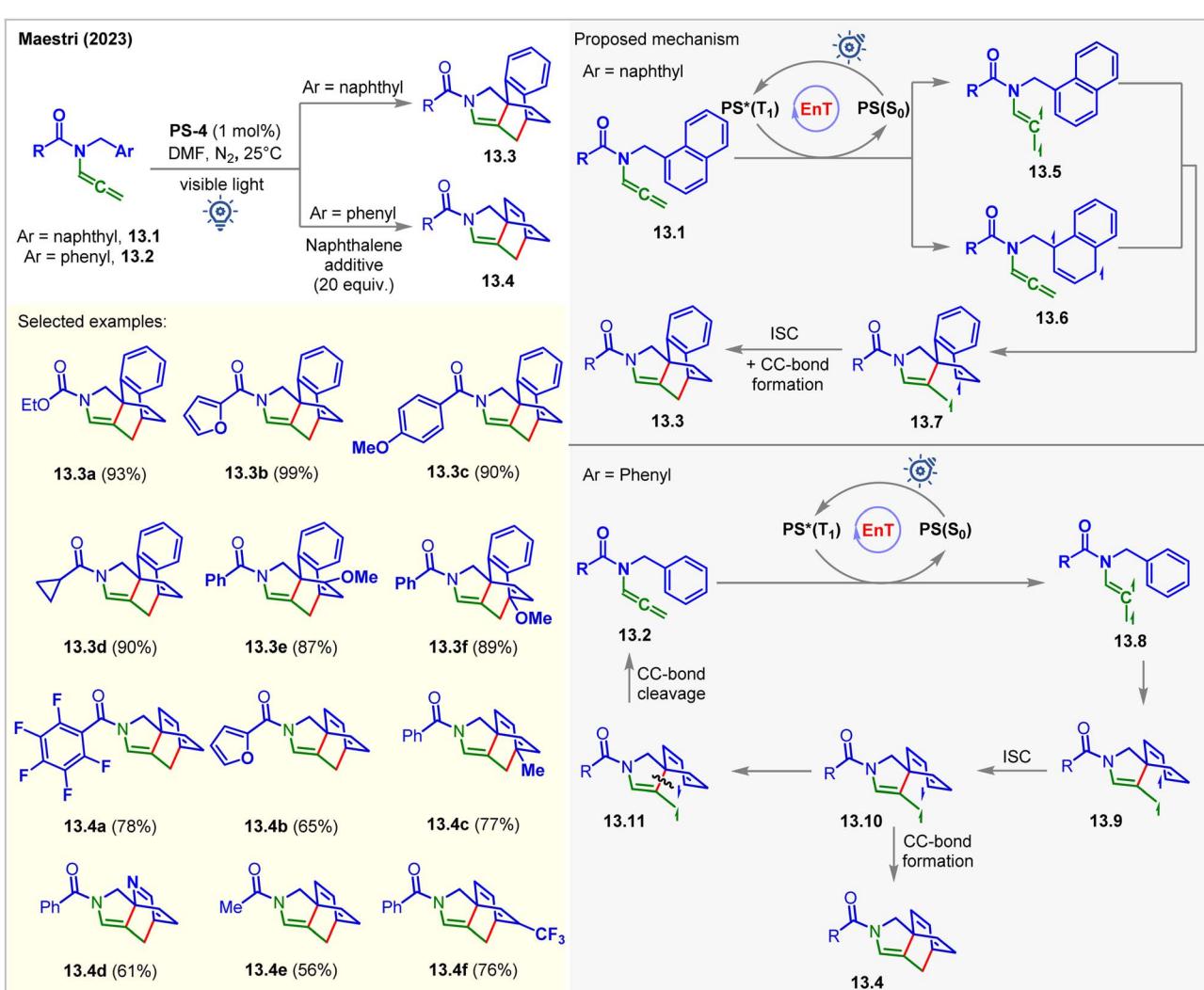
Fig. 13 Visible light mediated EnT dearomative intramolecular [4π + 2π] cycloaddition of allenamide tethered arenes.

cycloadducts **13.4**. An alternative pathway where the cleavage of a CC-bond of **13.10** occurs regenerating the starting material. Interestingly, this pathway is kinetically favored by 0.2 kcal mol^{-1} relative to the one derived for the radical addition. Computational studies at the M06/def2/TZVP level of theory were carried out for the mechanistic investigations. As a result of this unwanted side reaction, lower yields were obtained. Notably, the authors employed an excess of naphthalene as an additive to stabilize the biradical intermediate and the productive transition state *via* π-cloud interaction with the substrate. The yields were significantly improved under these conditions.

3.2. Intermolecular [4π + 2π] *para*-cycloaddition

In 2021, in collaboration, Glorius, Brown, and Houk established Brønsted and Lewis acid-assisted dearomative [4 + 2] cycloaddition of quinolines **14.1** with olefins *via* visible-light EnT catalysis (Fig. 14A).[99] The authors introduced two different conditions for differently substituted quinoline derivatives: condition A: **PS-2** (2 mol%) in HFIP, and condition B: **PS-2** (1 mol%) in CH$_2$Cl$_2$ with BF$_3$·OEt$_2$ (1 equiv.). The dearomative cycloaddition of 6-methyl quinoline with 1-hexene under condition A forms the cycloadduct **14.3a** in 88% yield with >95 : 5 dr as the only regioisomer. Whereas the reaction of the unsubstituted quinoline under condition B yields the cycloadduct **14.4a** in 78% yield with 83 : 17 dr as the major regioisomer with 18% of other regioisomers **14.3**. Condition A performed well for 5-, 6-, 7-, and 8-substituted quinolines. Anti-regioselectivity was observed for 2-, 3-, 4-, 5-, and 7-substituted quinolines, whereas 6-, and 8-substituted quinolines gave syn regioselectivity. No conversion occurred without HFIP and BF$_3$·OEt$_2$ in two separate reaction setups, indicating the requirement of either the Brønsted acid or the Lewis acid in achieving the desired cycloaddition reaction. Based on these findings, the authors proposed that the HFIP solvent and the BF$_3$·OEt$_2$ additive were adhering to the quinoline *via* hydrogen bonding and Lewis acid–base interaction, which lowers E_T of 6-methyl quinoline from 61.7 kcal mol^{-1} to 61.2 kcal mol^{-1} (in HFIP), and to 58.9 kcal mol^{-1} (with BF$_3$·OEt$_2$), respectively, which was supported by the ωB97X-D/6-311++G(d,p) level of computational study.

Independently, Morofuji reported the same reaction under similar conditions (Fig. 14B).[100] It was shown that adding triflic acid sped up the [4 + 2] cycloaddition reaction for the less reactive 5- or 8- substituted quinolines. The addition of acid increases the electrophilic nature of quinoline and helps to accelerate the reaction. Besides, upon protonation, the E$_T$s of lepidine decreased (to 56.4 from 59.1 kcal mol^{-1} of free lepidine). However, by performing a laser flash photolysis experiment, the authors found that the transfer of the PS's triplet energy to both neutral and cationic quinoline substrates produced the triplet state of quinoline **14.12(T$_1$)**. The Stern–Volmer experiments portrayed the quenching of **PS-2** by both the neutral quinoline derivative and cationic quinoline derivative **14.11**. It was suspected that the acceleration of EnT might not be the exact function of acids but to enhance the reactivity

of the triplet state of quinolines toward olefins. The authors concluded that the highly electron-rich nature of the biradical intermediate produced from a neutral quinoline moiety was the reason for its slow reaction with its olefin partner. The DFT calculations at the (U)-B3LYP/6-311G+(d,p) level of theory suggested that the cycloaddition pathway of neutral lepidine involves a high Gibbs energy barrier, which is responsible for no product formation.

In 2022, Brown, Glorius, Chen, and Houk expanded the substrate scope to disubstituted alkenes **14.16** and allenes **14.19** (Fig. 14C) for the Lewis acid-mediated [4 + 2] cycloaddition of quinolines *via* visible light EnT catalysis.[101] 5-Alkene-tethered quinoline also underwent [4 + 2] cycloaddition effortlessly to produce **14.17d**, leaving the tethered olefin intact. This indication was sufficient to realize the faster intermolecular reaction over the intramolecular reaction due to the slow radical addition step between C8 and the terminal carbon center of the tethered alkene forming an 8- or 9-membered transition state. The reaction of 5-alkyl quinolines **14.15** with styrene derivatives were observed to form an *endo* product **14.17** with high diastereoselectivity (up to >10 : 1 dr) due to the London dispersion force. The regioselectivity to form 8-to-5 products **14.17** were decided by the relative stability of the long-lived biradical intermediates. In comparison, a more polar solvent favored 5-to-8 products **14.18**. Allenes **14.19** also underwent cycloaddition with 5-alkyl quinolines **14.15** to exclusively produce 8-to-5 [4 + 2] cycloadducts **14.20**.

In 2023, the Guin group demonstrated a similar dearomative intermolecular [4 + 2] cycloaddition of lepidines **14.5** with alkenes **14.2** in the presence of 1.5 equiv. CF$_3$CO$_2$H as an additive (Fig. 14D).[102] **PS-2** (1 mol%) catalyzed the reaction in dichloroethane solvent under irradiation of blue LEDs. Notably, the reaction was moisture- and air-tolerant, giving the product **14.21** with up to 91% isolated yield and up to 19 : 1 dr.

In 2022, the Maji group commenced the intermolecular dearomative [4 + 2] cycloaddition of aromatic hydrocarbon 2-acetyl naphthalenes **15.1** with styrenes **15.2** employing **PS-2** (1 mol%) as the photocatalyst in acetonitrile at room temperature (Fig. 15A).[103] The bicyclo[2.2.2]octa-2,5-diene derivative **15.3a** was isolated as a single regioisomer in 98% yield with 2 : 1 dr favoring the *endo* diastereomer. The EnT from the excited photocatalyst **PS-2** (E_T = 61.8 kcal mol^{-1}) to naphthalene derivatives **15.1** (E_T = 55.1 kcal mol^{-1}) is exergonic and more favorable compared to the energy transfer to the styrene (E_T = 57.9 kcal mol^{-1}) moiety. The triplet energy values of **15.1** and **15.2** were calculated at the B3LYP/6-311+G(2d,p) level of DFT. The Stern–Volmer quenching study validated this fact (k_q(**15.1**) = 1.60 × 10^4 M^{-1} s^{-1} *vs.* k_q(**15.2**) = 0.41 × 10^4 M^{-1} s^{-1}). A styrene moiety with both EDG and EWG substitutions at the aryl group underwent cycloaddition with the same productivity.

Independently, Brown reported a similar reaction using [Ir(p-CF$_3$-ppy)$_3$] (**PS-12**, E_T = 56.4 kcal mol^{-1}) as the PS (Fig. 15A).[104] It was observed that the ester and amide-substituted naphthalenes did not undergo cycloaddition using **PS-2**. However, a promising result was shown when employing **PS-12**. This reaction was also extended to activated olefins bearing EWG groups, including cyano, ester, and ketones. The
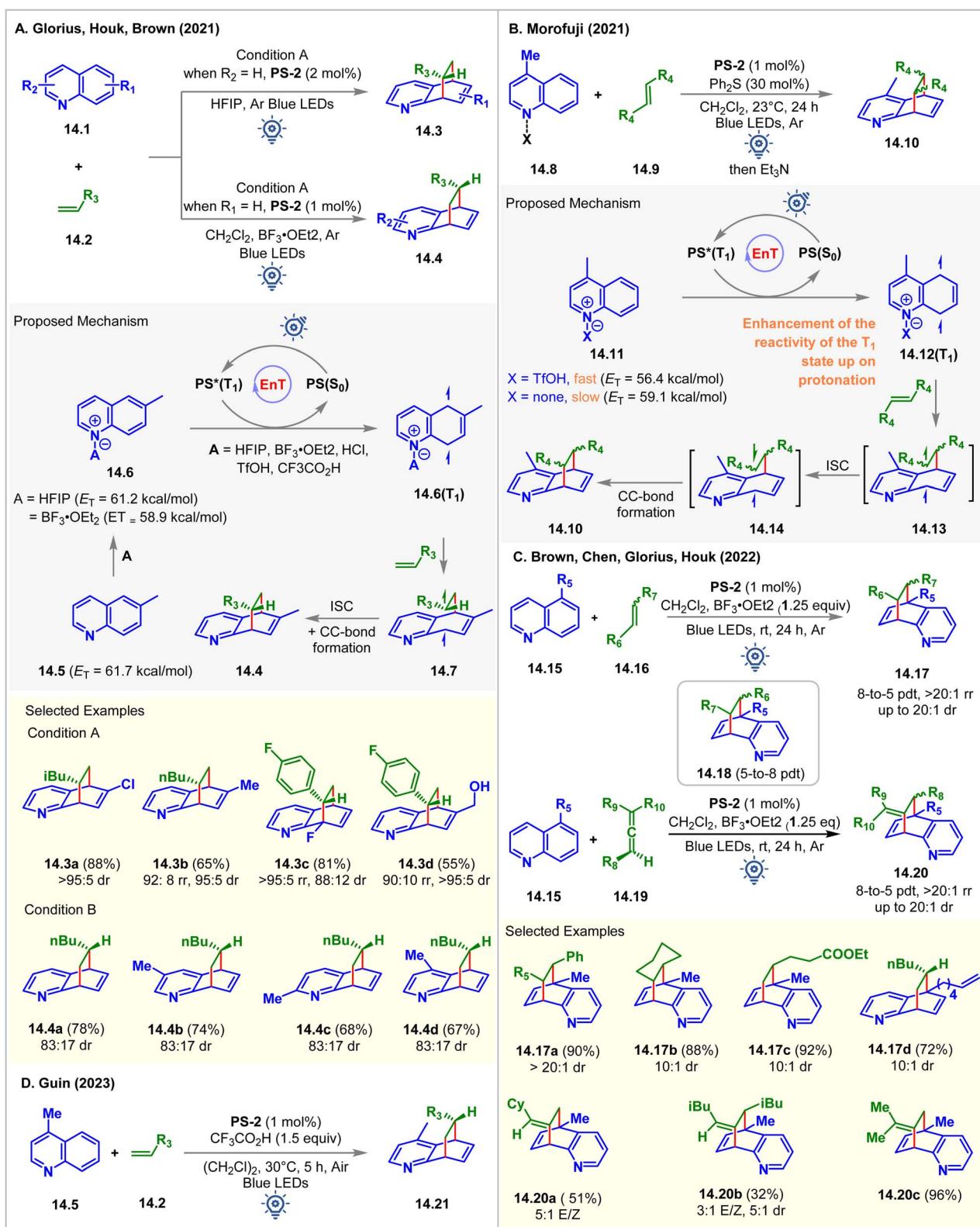
Fig. 14 Visible light mediated EnT dearomative intermolecular [4π + 2π] cycloaddition of (A) quinolines with olefins using Lewis acid and HFIP solvent, (B) quinoline with disubstituted olefins using TfOH, (C) quinolines with disubstituted olefins and allene usings lewis acid, and (D) lepidine with olefins using CF₃CO₂H.
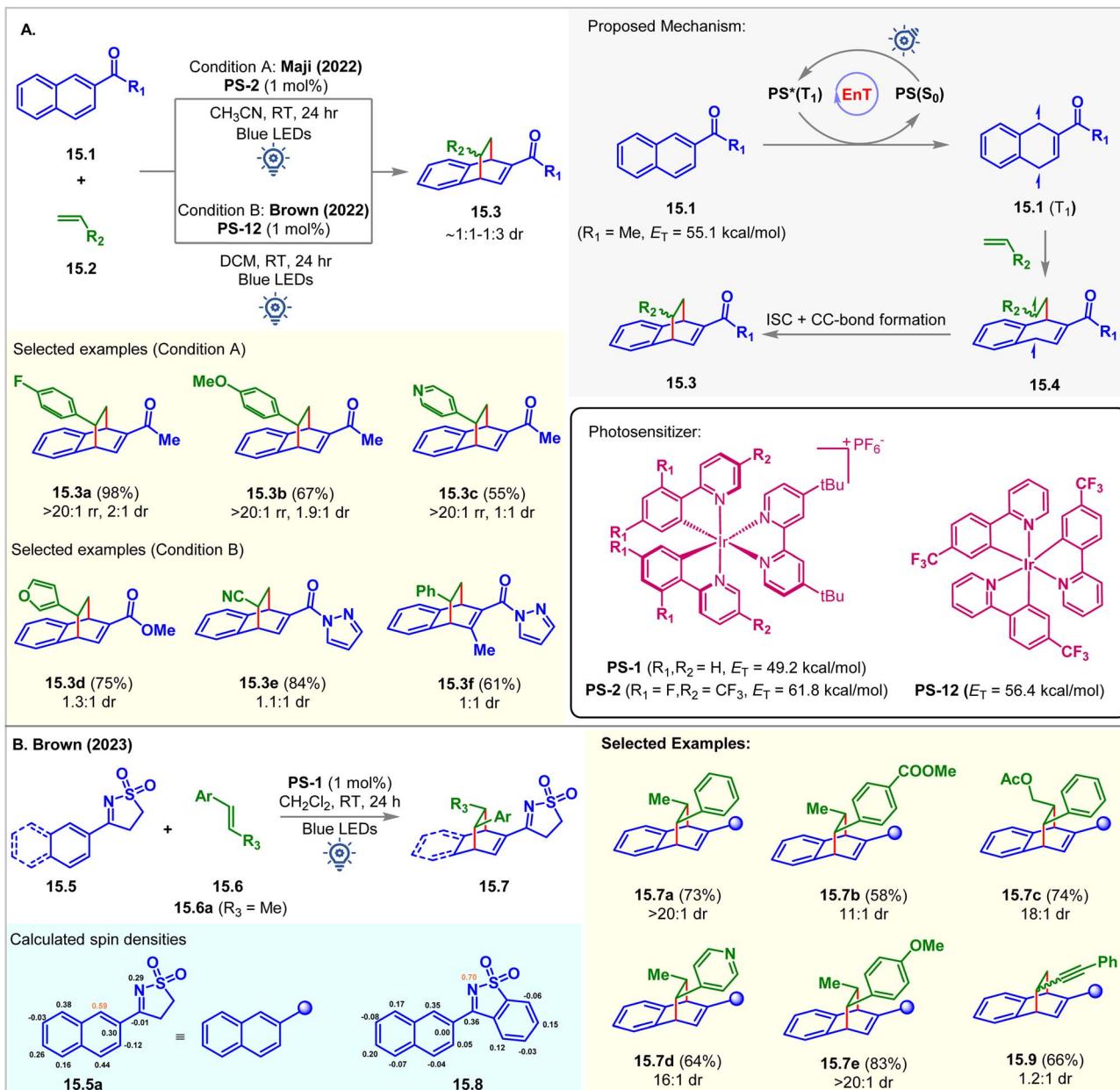
Fig. 15 Visible light mediated EnT dearomative intermolecular [4π + 2π] cycloaddition of (A) 2-COR-naphthalenes and (B) naphthyl tethered rigid sulfonylimine derivatives.

authors also found that the reaction proceeded well in the absence of PS upon irradiation with 365 nm LEDs, suggesting that the reaction proceeded *via* excited state triplet intermediates. Although good regioselectivity was obtained, the diastereoselectivity was poor (∼1 : 1 dr). Recently, the Brown group carried out further study to overcome the low diastereoselectivity challenge using a sulfonyl amine activating group (Fig. 15B).[105] Introduction of a larger activating group could distinguish two diastereomeric transition states to achieve high diastereoselectivity. Rigid sulfonylimines **15.5** underwent dearomative [4 + 2] cycloaddition with β-methyl styrene **15.6a** under blue LED irradiation of **PS-12** to produce cycloadduct **15.7a** with 73% yield and >20 : 1 dr. Electron donating and withdrawing

groups at the aryl ring of **15.6** provided excellent diastereoselectivity of for the [4 + 2] cycloadducts **15.7e** and **15.7b**, respectively. Alkenyl heterocycle also undergoes cycloaddition to achieve **15.7d** with excellent 16 : 1 dr. Interestingly, the derivatives of benzoisothiazole **15.8** undergo [2 + 2] cycloaddition with styrene to produce azetidine in a single diastereomer under 450 nm blue LED irradiation of **PS-12**. Spin density calculation of the excited triplet state of **15.5a** and **15.8** revealed the highest spin density at C1 of *N*-aryl sulfonylimine **15.5a** and the *N*-atom of benzoisothiazole derivative **15.8**, which correlates with the bond-formation sites and supports the behavior of the cycloaddition reaction.
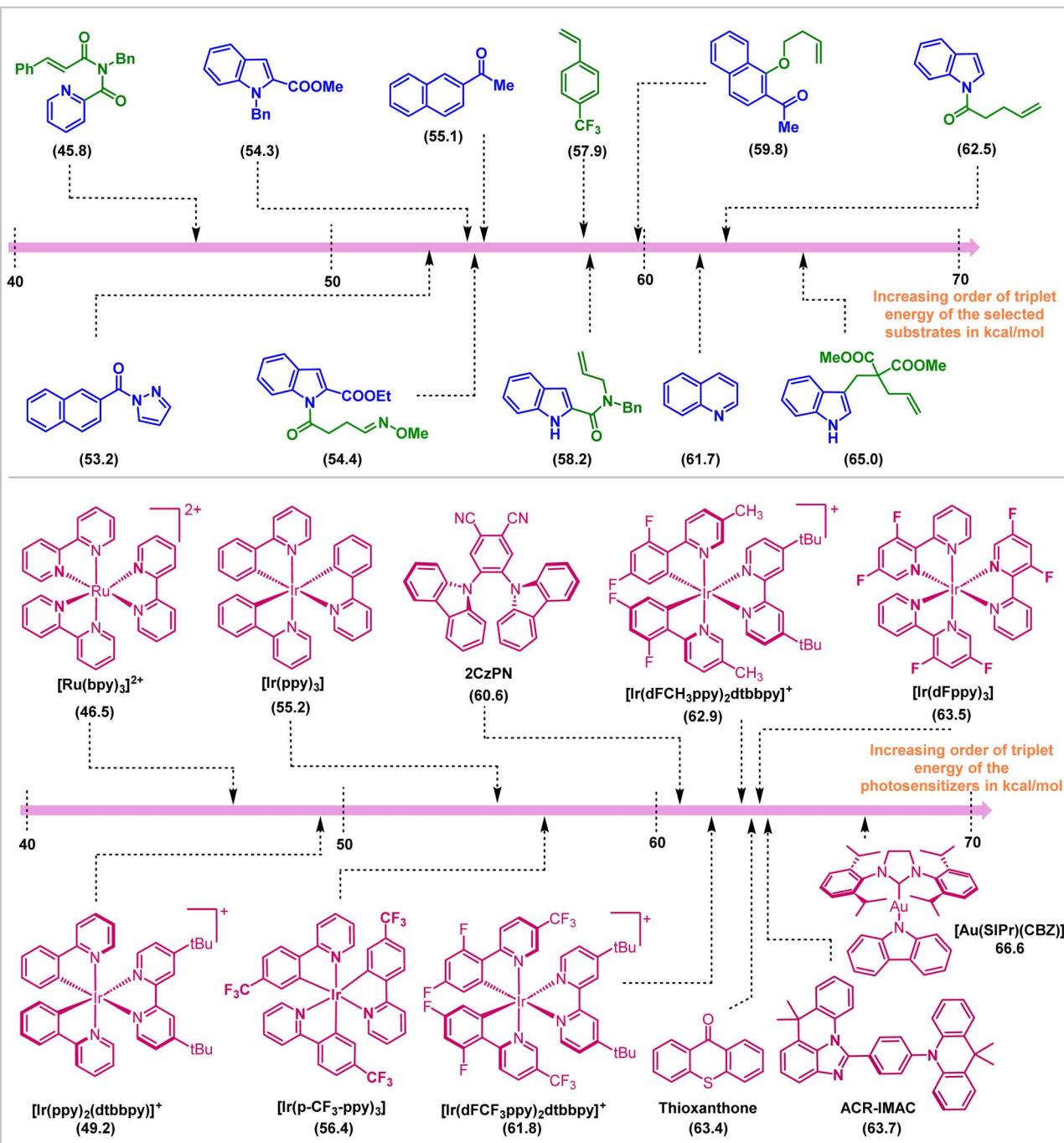
Fig. 16 Photosensitizers and substrates and their E_Ts (in kcal mol^{-1}, shown in parentheses) employed in visible-light mediated dearomative cycloaddition reactions.

4. Conclusion and outlook

In conclusion, this review covers the applications of visible light EnT catalysis in dearomative cycloaddition reactions. Appropriate choice of photosensitizer and reaction conditions enables direct and selective activation of the substrate molecules employing visible light sources (Fig. 16). The mildness of the protocol allowed the isolation of endergonic products in high yield and selectivities. Initial work in this field employed intramolecular reactions to compensate for entropic issues and the high reactivity and low lifetime of the visible light-activated substrates. Subsequent development allowed the discovery of intermolecular reactions, even the enantioselective variants. This advancement in the field of triplet-energy photosensitized dearomative cycloadditions is not only restricted to the π-based systems, but the recent inclusion of the σ-frameworks (for instance, BCBs) has also ensured the expansion of its horizon.

The synthetic work parallels experimental and computational mechanistic understanding of reactivity and selectivity.

Despite significant advances in this field, visible light induced EnT dearomatization reactions are still in their early stages. There are still substantial challenges and underexplored directions that continue to arouse more interest in the field. For instance, most EnT-induced dearomative cycloaddition reactions are involved in racemic product formations, and, except for one example, the asymmetric variants of such reactions are yet to be explored. Moreover, some of the reactions are less diastereoselective. Hence, modulation of the reaction parameters and improving the catalysis to address these selectivity issues would be one of the subjects of future research. Additionally, only a limited section of arenes are considered thus far. The challenges are not only accessing their excited states but also enabling their productive reactions with the coupling partners. A more interesting and widely applicable strategy is to design photosensitizers with higher triplet excited state energies that will allow activation of these recalcitrant molecules for functionalization reactions, as well as to redesign the existing substrates to reduce the triplet energy. Another important direction of such an EnT reaction should also be towards [3 + 2] cycloaddition reactions, which are yet to be performed under visible-light irradiation. Late-stage modification of drug molecules and their application in the total synthesis is a worthwhile future direction. We expect that the insights gained in this field to date, elaborated in this tutorial review, will provide an informative tool to aid the development of this emerging triplet energy transfer catalysis for selective transformative innovation.

Author contributions

All authors have given approval to the final version of the paper.

Conflicts of interest

The authors declare no competing financial interest.

Acknowledgements

References

1 W. Carruthers, *Cycloaddition Reactions in Organic Synthesis*, Elsevier Science, 2013.
2 S. Kobayashi and K. A. Jorgenson, in *Cycloaddition Reactions in Organic Synthesis*, Wiley-VCH Verlag GmbH, 2001, pp. 1–329.
3 R. Remy and C. G. Bochet, *Chem. Rev.*, 2016, **116**, 9816–9849.
4 U. Streit and C. G. Bochet, *Chimia*, 2008, **62**, 962–966.
5 D. Chappell, A. T. Russell and B. Chemistry, *Org. Biomol. Chem.*, 2006, **4**, 4409–4430.
6 J. Mattay, *Angew. Chem., Int. Ed.*, 2007, **46**, 663–665.
7 C. W. Bird, *Tetrahedron*, 1996, **52**, 9945–9952.
8 N. Hoffmann, *Chem. Rev.*, 2008, **108**, 1052–1103.
9 L. D. Elliott, S. Kayal, M. W. George and K. Booker-Milburn, *J. Am. Chem. Soc.*, 2020, **142**, 14947–14956.
10 D. Bryce-Smith, *Pure Appl. Chem.*, 1968, **16**, 47–64.
11 H. J. F. Angus and D. Bryce-Smith, *Proc. Chem. Soc.*, 1959, 326–327.
12 K. E. Wilzbach and L. Kaplan, *J. Am. Chem. Soc.*, 1966, **88**, 2066–2067.
13 K. E. Wilzbach and L. Kaplan, *J. Am. Chem. Soc.*, 1971, **93**, 2073–2074.
14 D. Bryce-Smith, *J. Chem. Soc. D*, 1969, 806–808.
15 K. N. Houk, *Pure Appl. Chem.*, 1982, **54**, 1633–1650.
16 R. B. Woodward and R. Hoffmann, *Angew. Chem., Int. Ed.*, 1969, **8**, 781–853.
17 W. Ferree Jr, J. B. Grutzner and H. Morrison, *J. Am. Chem. Soc.*, 1971, **93**, 5502–5512.
18 U. Streit and C. G. Bochet, *Beilstein J. Org. Chem.*, 2011, **7**, 525–542.
19 F. Mueller and J. Mattay, *Chem. Rev.*, 1993, **93**, 99–117.
20 J. Mattay, *Tetrahedron*, 1985, **41**, 2405–2417.
21 I. Yoshihisa, N. Katsuyuki, I. Koichi, H. Tadao and N. J. Turro, *Chem. Lett.*, 1982, **11**, 471–474.
22 D. C. Blakemore and A. Gilbert, *J. Chem. Soc., Perkin Trans. 1*, 1992, 2265–2270.
23 Q.-Q. Zhou, Y.-Q. Zou, L.-Q. Lu and W.-J. Xiao, *Angew. Chem., Int. Ed.*, 2019, **58**, 1586–1604.
24 F. Strieth-Kalthoff, C. Henkel, M. Teders, A. Kahnt, W. Knolle, A. Gómez-Suárez, K. Dirian, W. Alex, K. Bergander, C. G. Daniliuc, B. Abel, D. M. Guldi and F. Glorius, *Chem*, 2019, **5**, 2183–2194.
25 N. J. Turro, *Modern Molecular Photochemistry*, University Science Books, 1991.
26 D. L. Dexter, *J. Chem. Phys.*, 1953, **21**, 836–850.
27 P. Klán and J. Wirz, in *Photochemistry of Organic Compounds*, Wiley, Chichester, 2009, pp. 44–75.
28 S. L. Murov, I. Carmichael and G. L. Hug, *Handbook of Photochemistry*, New York, 1993.
29 V. Balzani, P. Ceroni and A. Juris, *Photochemistry and Photophysics: Concepts, Research, Applications*, John Wiley & Sons, 2014.
30 P. J. Wagner, Topics in current chemistry, *Top. Curr. Chem.*, 1976, 1–52.
31 C. K. Prier, D. A. Rankic and D. W. C. MacMillan, *Chem. Rev.*, 2013, **113**, 5322–5363.
32 J. Großkopf, T. Kratz, T. Rigotti and T. Bach, *Chem. Rev.*, 2022, **122**, 1626–1653.
33 F. Strieth-Kalthoff and F. Glorius, *Chem*, 2020, **6**, 1888–1903.
34 D. S. Lee, V. K. Soni and E. J. Cho, *Acc. Chem. Res.*, 2022, **55**, 2526–2541.
35 Y. Zhang, M. Xia, M. Li, Q. Ping, Z. Yuan, X. Liu, H. Yin, S. Huang and Y. Rao, *J. Org. Chem.*, 2021, **86**, 15284–15297.
36 Y. Matsushita, R. Ochi, Y. Tanaka, T. Koike and M. Akita, *Org. Chem. Front.*, 2020, **7**, 1243–1248.
37 Y. Zhang, Y. Zhang, C. Ye, X. Qi, L.-Z. Wu and X. Shen, *Nat. Commun.*, 2022, **13**, 6111–6121.

38 M. Bera, D. S. Lee and E. J. Cho, *Trends Chem.*, 2021, **3**, 877–891.

39 T. Rigotti and J. Alemán, *Chem. Commun.*, 2020, **56**, 11169–11190.

40 P. Franceschi, S. Cuadros, G. Goti and L. Dell'Amico, *Angew. Chem., Int. Ed.*, 2023, **62**, e202217210.

41 J. J. McCullough, W. K. MacInnis, C. J. L. Lock and R. Faggiani, *J. Am. Chem. Soc.*, 1980, **102**, 7780–7782.

42 Y. Hanzawa and L. Paquette, *Synth.*, 1982, 661–662.

43 P. J. Wagner and K. Nahm, *J. Am. Chem. Soc.*, 1987, **109**, 4404–4405.

44 N. Zupančič and B. Šket, *J. Chem. Soc., Perkin Trans. 1*, 1992, 179–180.

45 N. Hoffmann and J.-P. Pete, *Tetrahedron Lett.*, 1996, **37**, 2027–2030.

46 J. C. Namyslo and D. E. Kaufmann, *Chem. Rev.*, 2003, **103**, 1485–1538.

47 N.-Y. Fu, S.-H. Chan and H. N. C. Wong, in *The Chemistry of Cyclobutanes*, John Wiley & Sons, Ltd, 2005, pp. 357–440.

48 M. J. James, J. L. Schwarz, F. Strieth-Kalthoff, B. Wibbeling and F. Glorius, *J. Am. Chem. Soc.*, 2018, **140**, 8624–8628.

49 M. Zhu, C. Zheng, X. Zhang and S.-L. You, *J. Am. Chem. Soc.*, 2019, **141**, 2636–2644.

50 E. A. Martynova, V. A. Voloshkin, S. G. Guillet, F. Bru, M. Beliš, K. Van Hecke, C. S. J. Cazin and S. P. Nolan, *Chem. Sci.*, 2022, **13**, 6852–6857.

51 Z. Zhang, D. Yi, M. Zhang, J. Wei, J. Lu, L. Yang, J. Wang, N. Hao, X. Pan, S. Zhang, S. Wei and Q. Fu, *ACS Catal.*, 2020, **10**, 10149–10156.

52 M. Zhu, X. Zhang, C. Zheng and S.-L. You, *ACS Catal.*, 2020, **10**, 12618–12626.

53 M. Zhu, X.-L. Huang, H. Xu, X. Zhang, C. Zheng and S.-L. You, *CCS Chem.*, 2021, **3**, 652–664.

54 T. Hudlicky and J. W. Reed, *Angew. Chem., Int. Ed.*, 2010, **49**, 4864–4876.

55 P. Li, J. Zhao, L. Shi, J. Wang, X. Shi and F. Li, *Nat. Commun.*, 2018, **9**, 1972–1980.

56 M. Zhu, X.-L. Huang, S. Sun, C. Zheng and S.-L. You, *J. Am. Chem. Soc.*, 2021, **143**, 13441–13449.

57 M. S. Oderinde, E. Mao, A. Ramirez, J. Pawluczyk, C. Jorge, L. A. M. Cornelius, J. Kempson, M. Vetrichelvan, M. Pitchai, A. Gupta, A. K. Gupta, N. A. Meanwell, A. Mathur and T. G. M. Dhar, *J. Am. Chem. Soc.*, 2020, **142**, 3094–3103.

58 E. R. Sauvé, D. M. Mayder, S. Kamal, M. S. Oderinde and Z. M. Hudson, *Chem. Sci.*, 2022, **13**, 2296–2302.

59 A. B. Rolka and B. Koenig, *Org. Lett.*, 2020, **22**, 5035–5040.

60 N. Arai and T. Ohkuma, *Org. Lett.*, 2019, **21**, 1506–1510.

61 J. Proessdorf, C. Jandl, T. Pickl and T. Bach, *Angew. Chem., Int. Ed.*, 2022, **61**, e202208329.

62 N. Hu, H. Jung, Y. Zheng, J. Lee, L. Zhang, Z. Ullah, X. Xie, K. Harms, M.-H. Baik and E. Meggers, *Angew. Chem., Int. Ed.*, 2018, **57**, 6242–6246.

63 M. S. Oderinde, A. Ramirez, T. G. M. Dhar, L. A. M. Cornelius, C. Jorge, D. Aulakh, B. Sandhu, J. Pawluczyk, A. A. Sarjeant, N. A. Meanwell, A. Mathur and J. Kempson, *J. Org. Chem.*, 2021, **86**, 1730–1747.

64 P. K. Mykhailiuk, *Org. Biomol. Chem.*, 2019, **17**, 2839–2849.

65 M. A. M. Subbaiah and N. A. Meanwell, *J. Med. Chem.*, 2021, **64**, 14046–14128.

66 M. Golfmann and J. C. L. Walker, *Commun. Chem.*, 2023, **6**, 9–21.

67 M. A. A. Walczak, T. Krainz and P. Wipf, *Acc. Chem. Res.*, 2015, **48**, 1149–1158.

68 W. J. Leigh, *Chem. Rev.*, 1993, **93**, 487–505.

69 R. Kleinmans, T. Pinkert, S. Dutta, T. O. Paulisch, H. Keum, C. G. Daniliuc and F. Glorius, *Nature*, 2022, **605**, 477–482.

70 S. Agasti, F. Beltran, E. Pye, N. Kaltsoyannis, G. E. M. Crisenza and D. J. Procter, *Nat. Chem.*, 2023, **15**, 535–541.

71 R. Guo, Y.-C. Chang, L. Herter, C. Salome, S. E. Braley, T. C. Fessard and M. K. Brown, *J. Am. Chem. Soc.*, 2022, **144**, 7988–7994.

72 Y. Liu, S. Lin, Y. Li, J.-H. Xue, Q. Li and H. Wang, *ACS Catal.*, 2023, **13**, 5096–5103.

73 R. Kleinmans, S. Dutta, K. Ozols, H. Shao, F. Schäfer, R. E. Thielemann, H. T. Chan, C. G. Daniliuc, K. N. Houk and F. Glorius, *J. Am. Chem. Soc.*, 2023, **145**, 12324–12332.

74 H. Wang, H. Shao, A. Das, S. Dutta, H. T. Chan, C. Daniliuc, K. N. Houk and F. Glorius, *Science*, 2023, **381**, 75–81.

75 X. Jiang and R. Wang, *Chem. Rev.*, 2013, **113**, 5515–5546.

76 B. Yang and S. Gao, *Chem. Soc. Rev.*, 2018, **47**, 7926–7953.

77 J. A. Norton, *Chem. Rev.*, 1942, **31**, 319–523.

78 K. C. Nicolaou, S. A. Snyder, T. Montagnon and G. Vassilikogiannakis, *Angew. Chem., Int. Ed.*, 2002, **41**, 1668–1698.

79 M. Gregoritza and F. P. Brandl, *Eur. J. Pharm. Biopharm.*, 2015, **97**, 438–453.

80 K. N. Houk, *Acc. Chem. Res.*, 1975, **8**, 361–369.

81 S. J. Hamrock and R. S. Sheridan, *J. Am. Chem. Soc.*, 1989, **111**, 9247–9249.

82 A. Gilbert and G. Taylor, *J. Chem. Soc., Chem. Commun.*, 1978, 129–130.

83 D. Döpp, H. R. Memarian, C. Krüger and E. Raabe, *Chem. Ber.*, 1989, **122**, 585–588.

84 F. Birbaum, A. Neels and C. G. Bochet, *Org. Lett.*, 2008, **10**, 3175–3178.

85 T. W. Bingham, L. W. Hernandez, D. G. Olson, R. L. Svec, P. J. Hergenrother and D. Sarlah, *J. Am. Chem. Soc.*, 2019, **141**, 657–670.

86 W. C. Wertjes, M. Okumura and D. Sarlah, *J. Am. Chem. Soc.*, 2019, **141**, 163–167.

87 L. W. Hernandez, J. Pospech, U. Klöckner, T. W. Bingham and D. Sarlah, *J. Am. Chem. Soc.*, 2017, **139**, 15656–15659.

88 E. H. Southgate, J. Pospech, J. Fu, D. R. Holycross and D. Sarlah, *Nat. Chem.*, 2016, **8**, 922–928.

89 K. Ikeda, R. Kojima, K. Kawai, T. Murakami, T. Kikuchi, M. Kojima, T. Yoshino and S. Matsunaga, *J. Am. Chem. Soc.*, 2023, **145**, 9326–9333.

90 D. J. Bellville, D. W. Wirth and N. L. Bauld, *J. Am. Chem. Soc.*, 1981, **103**, 718–720.

91 D. J. Bellville, N. L. Bauld, R. Pabon and S. A. Gardner, *J. Am. Chem. Soc.*, 1983, **105**, 3584–3588.

92 M. Sicignano, R. I. Rodríguez and J. Alemán, *Eur. J. Org Chem.*, 2021, 3303–3321.

93 K. Kishikawa, S. Akimoto, S. Kohmoto, M. Yamamoto and K. Yamada, *J. Chem. Soc., Perkin Trans. 1*, 1997, 77–84.

94 L. Meites, P. Zuman and E. B. Rupp, *CRC handbook series in organic electrochemistry*, CRC Press, 1977.

95 J. Ma, F. Strieth-Kalthoff, T. Dalton, M. Freitag, J. L. Schwarz, K. Bergander, C. Daniliuc and F. Glorius, *Chem*, 2019, **5**, 2854–2864.

96 G. Zhen, G. Zeng, F. Wang, X. Cao and B. Yin, *Adv. Synth. Catal.*, 2023, **365**, 43–52.

97 M. Zhu, H. Xu, X. Zhang, C. Zheng and S.-L. You, *Angew. Chem., Int. Ed.*, 2021, **60**, 7036–7040.

98 M. Chiminelli, A. Serafino, D. Ruggeri, L. Marchiò, F. Bigi, R. Maggi, M. Malacria and G. Maestri, *Angew. Chem., Int. Ed.*, 2023, **62**, e202216817.

99 J. Ma, S. Chen, P. Bellotti, R. Guo, F. Schäfer, A. Heusler, X. Zhang, C. Daniliuc, M. K. Brown, K. N. Houk and F. Glorius, *Science*, 2021, **371**, 1338–1345.

100 T. Morofuji, S. Nagai, Y. Chitose, M. Abe and N. Kano, *Org. Lett.*, 2021, **23**, 6257–6261.

101 R. Guo, S. Adak, P. Bellotti, X. Gao, W. W. Smith, S. N. Le, J. Ma, K. N. Houk, F. Glorius, S. Chen and M. K. Brown, *J. Am. Chem. Soc.*, 2022, **144**, 17680–17691.

102 M. Bhakat, B. Khatua, P. Biswas and J. Guin, *Org. Lett.*, 2023, **25**, 3089–3093.

103 P. Rai, K. Maji, S. K. Jana and B. Maji, *Chem. Sci.*, 2022, **13**, 12503–12510.

104 W. Wang, Y. Cai, R. Guo and M. K. Brown, *Chem. Sci.*, 2022, **13**, 13582–13587.

105 W. Wang and M. K. Brown, *Angew. Chem., Int. Ed.*, 2023, e202305622.